Erratum: Subbarrier Fusion Reactions and Many-Particle Quantum Tunneling [Prog. Theo. Phys. 128 (2012) 1061]

Kouichi HAGINO[1] and Noboru TAKIGAWA[1,2]

[1]*Department of Physics, Tohoku University, Sendai 980-8578, Japan*
[2]*Tohoku Instiute of Technology, Sendai 982-8577, Japan*

We have found typographical errors in Eqs. (3.10), (3.36), (3.38), (3.41), (3.49), (B.8), and (B.10). These are corrected in the revised version given below. We thank K. Sannohe for pointing out these errors.

$$V^J_{\alpha lI;\alpha' l' I'}(r) = \langle (\alpha lI)JM|V_{\rm coup}(\boldsymbol{r},\xi)|(\alpha' l' I')JM\rangle, \tag{3·9}$$

$$= \sum_\lambda (-)^{l'+I+J} f_\lambda(r)\langle l||Y_\lambda||l'\rangle\langle \alpha I||T_\lambda||\alpha' I'\rangle \times \left\{ \begin{array}{ccc} J & I & l \\ \lambda & l' & I' \end{array} \right\}. \tag{3·10}$$

$$f_\lambda(r) = -R_T \frac{dV_N}{dr} + \frac{3}{2\lambda+1} Z_P Z_T e^2 \frac{R_T^\lambda}{r^{\lambda+1}}, \tag{3·36}$$

$$f_\lambda(R_b) = \frac{Z_P Z_T e^2}{R_b}\left(\frac{3}{2\lambda+1}\frac{R_T^\lambda}{R_b^\lambda} - \frac{R_T}{R_b}\right) \tag{3·38}$$

$$H_0 + V_{\rm coup} = \begin{pmatrix} 0 & F(r) & 0 \\ F(r) & \hbar\omega_\lambda & \sqrt{2}F(r) \\ 0 & \sqrt{2}F(r) & 2\hbar\omega_\lambda \end{pmatrix}, \tag{3·41}$$

$$H_0 + V_{\rm coup} = H_0 + f_2(r)\beta_2\langle Y_{I'0}|Y_{20}|Y_{I0}\rangle = \begin{pmatrix} 0 & F(r) & 0 \\ F(r) & \epsilon_2 + \frac{2\sqrt{5}}{7}F(r) & \frac{6}{7}F(r) \\ 0 & \frac{6}{7}F(r) & \frac{10}{3}\epsilon_2 + \frac{20\sqrt{5}}{77}F(r) \end{pmatrix} \tag{3·49}$$

$$\sigma_{\rm osc}(E) = 4\pi\mu R_b^2 \frac{\hbar\Omega}{k^2\hbar^2} \exp\left(-\frac{\pi\mu R_b^2\hbar\Omega}{l_g+\frac{1}{2}}\cdot\frac{1}{\hbar^2}\right)\sin(2\pi l_g). \tag{B·8}$$

$$\sigma_{\rm osc}(E) = 4\pi\mu R_b^2 \frac{\hbar\Omega}{k^2\hbar^2} \exp\left(-\frac{\pi\mu R_b^2\hbar\Omega}{2l_g+1}\cdot\frac{1}{\hbar^2}\right)\sin(\pi l_g). \tag{B·10}$$

Subbarrier Fusion Reactions and Many-Particle Quantum Tunneling

Kouichi HAGINO[1] and Noboru TAKIGAWA[1,2]

[1]*Department of Physics, Tohoku University, Sendai 980-8578, Japan*
[2]*Tohoku Instiute of Technology, Sendai 982-8577, Japan*

(Received September 28, 2012)

Low-energy heavy-ion fusion reactions are governed by quantum tunneling through the Coulomb barrier formed by the strong cancellation of the repulsive Coulomb force with the attractive nuclear interaction between the colliding nuclei. Extensive experimental as well as theoretical studies have revealed that fusion reactions are strongly influenced by couplings of the relative motion of the colliding nuclei to several nuclear intrinsic motions. Heavy-ion subbarrier fusion reactions thus provide a good opportunity to address the general problem of quantum tunneling in the presence of couplings, which has been a popular subject in recent decades in many branches of physics and chemistry. Here, we review theoretical aspects of heavy-ion subbarrier fusion reactions from the viewpoint of quantum tunneling in systems with many degrees of freedom. Particular emphases are put on the coupled-channels approach to fusion reactions and the barrier distribution representation for multichannel penetrability. We also discuss an application of the barrier distribution method to elucide the mechanism of the dissociative adsorption of H_2 molecules in surface science.

Subject Index: 062,211,223,226,330

§1. Introduction

Quantum mechanics is indispensable in understanding microscopic systems such as atoms, molecules, and atomic nuclei. One of its fundamental aspects is quantum tunneling, where a particle penetrates into a classically forbidden region. This is a wave phenomenon and is frequently encountered in diverse processes in physics and chemistry.

The importance of quantum tunneling has been recognized since the birth of quantum mechanics. For instance, it was as early as 1928 that Gamow, and independently Gurney and Condon, applied quantum tunneling to α decays of atomic nuclei and successfully explained the systematics of the experimental half-lives of radioactive nuclei.[1),2)]

In many applications of quantum tunneling, one only considers the penetration of a one-dimensional potential barrier, or a barrier with a single variable. In general, however, a particle which penetrates a potential barrier is never isolated but interacts with its surroundings or environment, resulting in modification in its behavior. Moreover, when the particle is a composite particle, quantum tunneling has to be discussed from a many-particle point of view. Quantum tunneling therefore inevitably takes place in reality in a multidimensional space. This problem was first addressed by Kapur and Peierls in 1937.[3)] Their theory has been further developed by, for example, Banks et al.,[4)] Gervais and Sakita,[5)] Brink et al.,[6)] Schmid,[7)] and

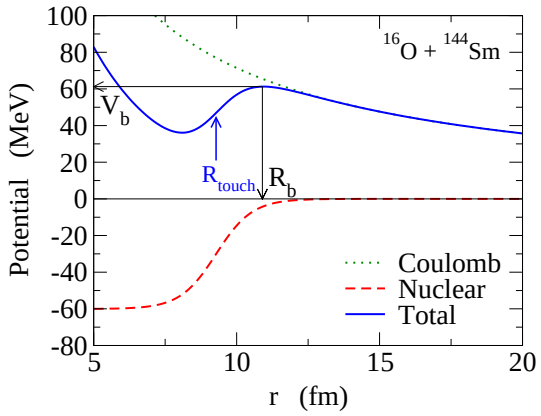

Fig. 1. Internucleus potential between ^{16}O and ^{144}Sm nuclei as a function of the relative distance. The dotted and dashed lines are the Coulomb and nuclear potentials, respectively, while the solid line denotes the total potential. V_b and R_b are the height and position of the Coulomb barrier, respectively. $R_{\rm touch}$ is the touching radius at which the projectile and target nuclei start overlapping significantly with each other.

Takada and Nakamura.[8)]

When quantum tunneling occurs in a complex system, such as the trapped flux in a superconducting quantum interference device (SQUID) ring,[9)] the tunneling variable couples to a large number of other degrees of freedom. In such systems, the environmental degrees of freedom more or less reveal a dissipative character. Quantum tunneling under the influence of dissipative environments plays an important role and is a fundamental problem in many fields of physics and chemistry. This problem has been studied in detail by Caldeira and Leggett.[10)] Their seminal work has stimulated many experimental and theoretical works, and has made quantum tunneling in systems with many degrees of freedom a topic of immense interest during recent decades.[11)]

In nuclear physics, one of the typical examples of tunneling phenomena is the heavy-ion fusion reaction at energies near and below the Coulomb barrier.[12),13)] Fusion is defined as a reaction in which two separate nuclei combine together to form a compound nucleus. In order for a fusion reaction to take place, the relative motion between the colliding nuclei has to overcome the Coulomb barrier formed by the strong cancellation between the long-range repulsive Coulomb and short-range attractive nuclear forces (as a typical example, Fig. 1 shows the internucleus potential between ^{16}O and ^{144}Sm nuclei as a function of the relative distance). Unless under extreme conditions, it is reasonable to assume that atomic nuclei are isolated systems and the couplings to external environments can be neglected. Nevertheless, one can still consider *intrinsic* environments. The whole spectra of excited states of the target and projectile nuclei (as well as several types of nucleon transfer processes) are populated in a complex way during fusion reactions. They act as environments to which the relative motion between the colliding nuclei couples. In fact, it has by now been well established that cross sections of heavy-ion fusion reactions are substantially enhanced owing to couplings to nuclear intrinsic degrees of freedom at

energies below the Coulomb barrier as compared with the predictions of a simple potential model.[12)–18)] Heavy-ion subbarrier fusion reactions thus make good examples of environment-assisted tunneling phenomena.

Theoretically, the standard way to address the effects of the couplings between the relative motion and nuclear intrinsic degrees of freedom on fusion reactions is to numerically solve the coupled-channels equations, which include all the relevant channels. In the eigenchannel representation of coupled-channels equations, the effects of channel coupling can be interpreted in terms of the distribution of fusion barriers.[13),19)–21)] In this representation, the fusion cross section is given by a weighted sum of the fusion cross sections for each eigenbarrier. The eigenbarriers lower than the original barrier are responsible for the enhancement of the fusion cross section at energies below the Coulomb barrier. On the basis of this idea, Rowley et al. have proposed a method to extract barrier distributions directly from experimental fusion excitation functions by taking the second derivative of the product of the fusion cross section and the center of mass energy $E\sigma_{\rm fus}$ with respect to E, i.e., $d^2(E\sigma_{\rm fus})/dE^2$.[22)] This method was tested against high-precision experimental data of fusion cross sections soon after it was proposed.[23)] The extracted fusion barrier distributions were sensitive to the effects of channel couplings and provided a much clearer way of understanding their effects on the fusion process than the fusion excitation functions themselves. It is now well recognized that the barrier distribution approach is a standard tool for heavy-ion subbarrier fusion reactions.[13),18)]

The aim of this paper is to review theoretical aspects of heavy-ion subbarrier fusion reactions from the viewpoint of the quantum tunneling of composite particles. To this end, we mainly base our discussions on the coupled-channels approach. Earlier reviews on the subbarrier fusion reactions can be found in Refs. 12)–16). See also Refs. 24) and 25) for reviews on subbarrier fusion reactions of radioactive nuclei, and Refs. 26) and 27) for reviews on fusion reactions relevant to the synthesis of superheavy elements, neither of which we cover in this article.

The paper is organized as follows. We will first discuss in the next section a potential model approach to heavy-ion fusion reactions. This is the simplest approach to fusion reactions, in which only elastic scattering and fusion are assumed to occur. This approach is adequate for light systems, but for fusion with a medium-heavy or heavy target nucleus the effects of nuclear excitations during fusion start playing an important role. In §3, we will discuss the effect of such a nuclear structure on heavy-ion fusion reactions. To this end, we will introduce and detail the coupled-channels formalism, which takes into account the inelastic scattering and transfer processes during fusion reactions. In §4, light will be shed on the fusion barrier distribution representation of the fusion cross section defined as $d^2(E\sigma_{\rm fus})/dE^2$. It is known that this approach is exact when the excitation energy of the intrinsic motion is zero, but we will demonstrate that one can also generalize it unambiguously using the eigenchannel approach to the case when the excitation energy is finite. In §5, we will discuss the present status of our understanding of deep-subbarrier fusion reactions. At these energies, fusion cross sections have been shown to be suppressed compared with the values obtained by standard coupled-channels calculations. This phenomenon may be related to dissipative quantum tunneling, that is, an irreversible

coupling to intrinsic degrees of freedom. In §6, we will discuss an application of the barrier distribution method to surface physics, more specifically, the effect of rotational excitations on the dissociative adsorption process of H_2 molecules. We will then summarize the paper in §7.

§2. One-dimensional potential model

2.1. *Ion-ion potential*

Theoretically, the simplest approach to heavy-ion fusion reactions is to use the one-dimensional potential model where both the projectile and the target are assumed to be structureless. The potential between the projectile and the target is given by a function of the relative distance r between them. It consists of two parts, that is,

$$V(r) = V_N(r) + V_C(r), \tag{2·1}$$

where $V_N(r)$ is the nuclear potential and $V_C(r)$ is the Coulomb potential, given by

$$V_C(r) = \frac{Z_P Z_T e^2}{r}, \tag{2·2}$$

in the outside region where the projectile and target nuclei do not significantly overlap with each other. Figure 1 shows a typical potential $V(r)$ for the s-wave scattering of the ^{16}O + ^{144}Sm reaction. The dotted and dashed lines are the nuclear and Coulomb potentials, respectively, while the total potential $V(r)$ is denoted by the solid line. One can see that a potential barrier appears owing to the strong cancellation between the short-range attractive nuclear interaction and the long-range repulsive Coulomb force. This potential barrier is referred to as the *Coulomb barrier* and has to be overcome in order for the fusion reaction to take place. $R_{\rm touch}$ in the figure is the touching radius, at which the projectile and target nuclei begin overlapping considerably. One can see that the Coulomb barrier is located outside the touching radius.

There are several ways to estimate the nuclear potential $V_N(r)$. One standard method is to fold a nucleon-nucleon interaction with the projectile and target densities.[28] The direct part of the nuclear potential in this double-folding procedure is given by

$$V_N(r) = \int d\boldsymbol{r}_1 d\boldsymbol{r}_2\, v_{NN}(\boldsymbol{r}_2 - \boldsymbol{r}_1 - \boldsymbol{r})\rho_P(\boldsymbol{r}_1)\rho_T(\boldsymbol{r}_2), \tag{2·3}$$

where v_{NN} is the effective nucleon-nucleon interaction, and ρ_P and ρ_T are the densities of the projectile and target, respectively. The double-folding potential is in general a nonlocal potential owing to the antisymmetrization effect of nucleons. Usually, either a zero-range approximation[28),29)] or a local momentum approximation[30)–34)] is employed in order to treat the nonlocality of the potential.

A phenomenological nuclear potential has also been employed. For instance, the Woods-Saxon form

$$V_N(r) = -\frac{V_0}{1 + \exp[(r - R_0)/a]}, \tag{2·4}$$

with

$$V_0 = 16\pi\gamma\bar{R}a, \tag{2·5}$$

$$R_0 = R_P + R_T, \tag{2·6}$$

$$R_i = 1.20A_i^{1/3} - 0.09 \text{ fm}, \qquad (i = P, T) \tag{2·7}$$

$$\bar{R} = R_P R_T/(R_P + R_T), \tag{2·8}$$

$$\gamma = 0.95\left[1 - 1.8\left(\frac{N_P - Z_P}{A_P}\right)\left(\frac{N_T - Z_T}{A_T}\right)\right] \text{ MeV fm}^{-2}, \tag{2·9}$$

$$1/a = 1.17\left[1 + 0.53\left(A_P^{-1/3} + A_T^{-1/3}\right)\right] \text{ fm}^{-1}, \tag{2·10}$$

has been widely used, where the parameters were determined from a least-squares fit to the experimental data of heavy-ion elastic scattering.[35),36)]

A nuclear potential thus constructed has been successful in reproducing experimental angular distributions of elastic and inelastic scattering for many systems. Moreover, the empirical value of the surface diffuseness parameter, $a \sim 0.63$ fm, is consistent with a double-folding potential. Recently, the value of the surface diffuseness parameter has been determined unambiguously using heavy-ion quasi-elastic scattering at deep-subbarrier energies.[37),38)] It has been confirmed that the experimental data are consistent with a value of around $a \sim 0.63$ fm.[38)–41)]

In marked contrast, recent experimental data for heavy-ion subbarrier fusion reactions suggest that a much larger value of the surface diffuseness parameter, ranging from 0.75 to 1.5 fm, is required to fit the data.[18),42)–46)] The Woods-Saxon potential which fits elastic scattering overestimates fusion cross sections at energies both above and below the Coulomb barrier, having an inconsistent energy dependence with the experimental fusion excitation function. The reason for the large discrepancies in the diffuseness parameters extracted from scattering and fusion analyses has not yet been fully understood. However, it is probably the case that the double-folding procedure is valid only in the surface region, while several dynamical effects come into play in the inner part, where fusion is sensitive to.

We summarize the relation between the surface diffuseness parameter a of a nuclear potential and the parameters of the Coulomb barrier, that is, the curvature, the barrier height, and the barrier position in Appendix A for exponential and Woods-Saxon potentials.

2.2. *Fusion cross sections*

In the potential model, the internucleus potential, $V(r)$, is supplemented by an imaginary part, $-iW(r)$, which mocks up the formation of a compound nucleus. One then solves the Schrödinger equation

$$\left[-\frac{\hbar^2}{2\mu}\frac{d^2}{dr^2} + V(r) - iW(r) + \frac{l(l+1)\hbar^2}{2\mu r^2} - E\right] u_l(r) = 0 \tag{2·11}$$

for each partial wave l, where μ is the reduced mass of the system, with the boundary conditions of

$$u_l(r) \sim r^{l+1}, \qquad r \to 0, \tag{2·12}$$

$$= H_l^{(-)}(kr) - S_l\, H_l^{(+)}(kr), \qquad r \to \infty. \tag{2·13}$$

Here, $H_l^{(+)}$ and $H_l^{(-)}$ are the outgoing and incoming Coulomb wave functions, respectively. S_l is the nuclear S-matrix and $k = \sqrt{2\mu E/\hbar^2}$ is the wave number associated with the energy E.

If the imaginary part of the potential, $W(r)$, is confined well inside the Coulomb barrier, one can regard the total absorption cross section as the fusion cross section, i.e.,

$$\sigma_{\rm fus}(E) \sim \sigma_{\rm abs}(E) = \frac{\pi}{k^2}\sum_l (2l+1)\left(1 - |S_l|^2\right). \tag{2·14}$$

In heavy-ion fusion reactions, instead of imposing the regular boundary condition at the origin, Eq. (2·12), the so-called incoming wave boundary condition (IWBC), is often applied without introducing the imaginary part of the potential, $W(r)$.[19),47)] Under the IWBC, the wave function has the form

$$u_l(r) = \sqrt{\frac{k}{k_l(r)}}\,\mathcal{T}_l \exp\left(-i\int_{r_{\rm abs}}^{r} k_l(r')dr'\right) \qquad r \le r_{\rm abs} \tag{2·15}$$

at a distance smaller than the absorption radius $r_{\rm abs}$, which is taken to be inside the Coulomb barrier. Here, $k_l(r)$ is the local wave number for the lth partial wave, defined by

$$k_l(r) = \sqrt{\frac{2\mu}{\hbar^2}\left(E - V(r) - \frac{l(l+1)\hbar^2}{2\mu r^2}\right)}. \tag{2·16}$$

The IWBC corresponds to the case where there is strong absorption in the inner region so that the incoming flux never returns. For heavy-ion fusion reactions, the final result is not sensitive to the choice of the absorption radius $r_{\rm abs}$, and the absorption radius is often taken to be at the pocket of the potential.[48)] With the IWBC, $\mathcal{T}_l$ in Eq. (2·15) is interpreted as the transmission coefficient. Equation (2·14) is then transformed to

$$\sigma_{\rm fus}(E) = \frac{\pi}{k^2}\sum_l (2l+1)P_l(E), \tag{2·17}$$

where $P_l(E)$ is the penetrability for the l-wave scattering, defined as

$$P_l(E) = 1 - |S_l|^2 = |\mathcal{T}_l|^2, \tag{2·18}$$

for the boundary conditions (2·13) and (2·15). The mean angular momentum of the compound nucleus is evaluated in a similar way as

$$\langle l\rangle(E) = \frac{\frac{\pi}{k^2}\sum_l l(2l+1)P_l(E)}{\frac{\pi}{k^2}\sum_l (2l+1)P_l(E)}. \tag{2·19}$$

For a parabolic potential, Wong has derived an analytic expression for fusion cross sections, Eq. (2·17).[49)] We will discuss this in Appendix B.

The IWBC, Eq. (2·15), has two advantages over the regular boundary condition, Eq. (2·12). The first advantage is that the imaginary part of the nuclear potential is

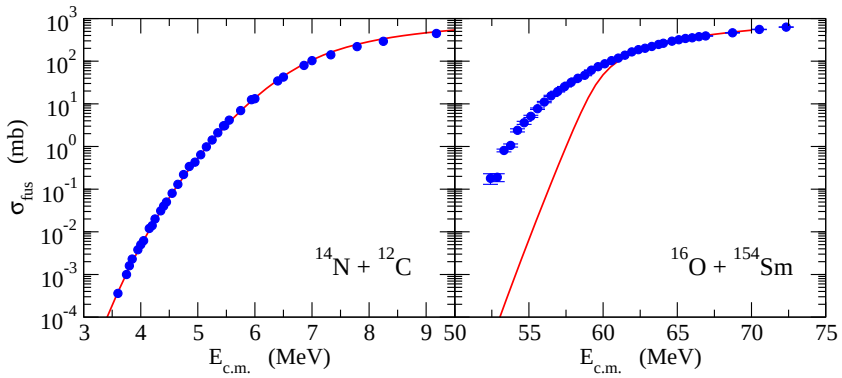

Fig. 2. Comparison of experimental fusion cross sections for the ^{14}N+^{12}C system (left panel) and ^{16}O+^{154}Sm system (right panel) with results of the potential model calculations (solid lines). The height of the Coulomb barrier is around $V_b \sim 6.9$ and 59 MeV for ^{14}N+^{12}C and ^{16}O+^{154}Sm, respectively. The experimental data are taken from Refs. 50) and 18) for the ^{14}N+^{12}C and ^{16}O+^{154}Sm reactions, respectively.

not needed, and the number of adjustable parameters can be reduced. The second point is that the IWBC directly provides the penetrability $P_l(E) = |\mathcal{T}_l|^2$ and thus the round-off error can be avoided in evaluating $1 - |S_l|^2$. This is a crucial point at energies well below the Coulomb barrier, where S_l is close to unity. Note that the IWBC does not necessarily correspond to the limit of $W(r) \to \infty$, as the quantum reflection due to $W(r)$ has to be neglected in order to realize it. The IWBC should thus be regarded as a different model from the regular boundary condition.

2.3. *Comparison with experimental data: success and failure of the potential model*

Let us now compare the one-dimensional potential model for the heavy-ion fusion reaction with experimental data. Figure 2 shows the experimental excitation functions of the fusion cross section for ^{14}N+^{12}C (left panel) and ^{16}O+^{154}Sm (right panel) systems, as well as results of the potential model calculation (solid lines). One can see that the potential model well reproduces the experimental data for the lighter system, ^{14}N + ^{12}C. On the other hand, the potential model apparently underestimates the fusion cross section for the heavier system, ^{16}O + ^{154}Sm, although it reproduces the experimental data at energies above the Coulomb barrier, which is about 59 MeV for this system.

To help understand the origin of the failure of the potential model, Fig. 3 shows the experimental fusion excitation functions for the ^{16}O + ^{144,148,154}Sm reactions[18] and a comparison with the potential model (solid line). To remove the trivial target dependence, data are plotted as a function of the center of mass energy relative to the barrier height for each system, and the fusion cross sections are divided by the geometrical factor, πR_b^2. With these prescriptions, the fusion cross sections for the different systems match each other at energies above the Coulomb barrier, although one can also consider a more refined prescription.[51),52)] The barrier height and the result of the potential model are obtained with the Akyüz-Winther potential.[36)] One again observes that the experimental fusion cross sections are drastically enhanced

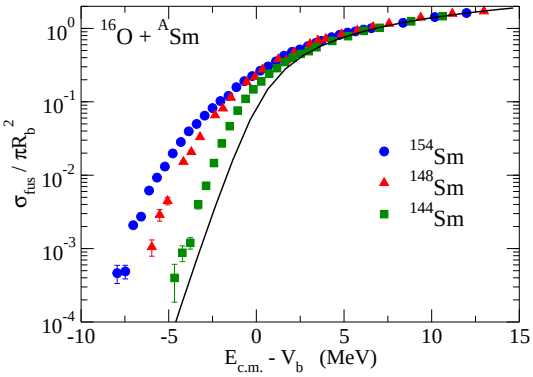

Fig. 3. Experimental fusion cross sections for ^{16}O+^{144,148,154}Sm systems, taken from Ref. 18). In order to remove the trivial target dependence, the experimental fusion cross sections are divided by πR_b^2, where R_b is the position of the Coulomb barrier, and the energies are measured with respect to the barrier height, V_b, for each system. The solid line shows the result of the potential model calculation.

at energies below the Coulomb barrier compared with the prediction of the potential model. Moreover, one also observes that the degree of enhancement of the fusion cross section depends strongly on the target nucleus. That is, the enhancement for the ^{16}O + ^{154}Sm system is several order of magnitude, while that for the ^{16}O + ^{144}Sm system is about a factor of four at energies below the Coulomb barrier. This strong target dependence of fusion cross sections suggests that low-lying collective excitations play a role, as we will discuss in the next section.

The inadequacy of the potential model has been demonstrated in a more transparent way by Balantekin et al.[53] Within the semi-classical approximation, the penetrability for a one-dimensional barrier can be inverted to yield the barrier thickness.[54] Balantekin et al. applied such an inversion formula directly to experimental fusion cross sections in order to construct an effective internucleus potential. Assuming a one-dimensional energy-independent local potential, the resultant potentials were unphysically thin for heavy systems, often with a multivalued potential. This result was also confirmed by the systematic study in Ref. 55). These analyses have provided clear evidence for the inadequacy of the one-dimensional barrier passing model for heavy-ion fusion reactions, and has triggered the development of the coupled-channels approach, which we will discuss in the next section.

In passing, we have recently applied the inversion procedure in a modified way to determine the lowest potential barrier among the distributed barriers due to the effects of channel coupling.[56] The extracted potential for ^{16}O + ^{208}Pb scattering is well behaved, indicating that the channel coupling indeed plays an essential role in subbarrier fusion reactions.

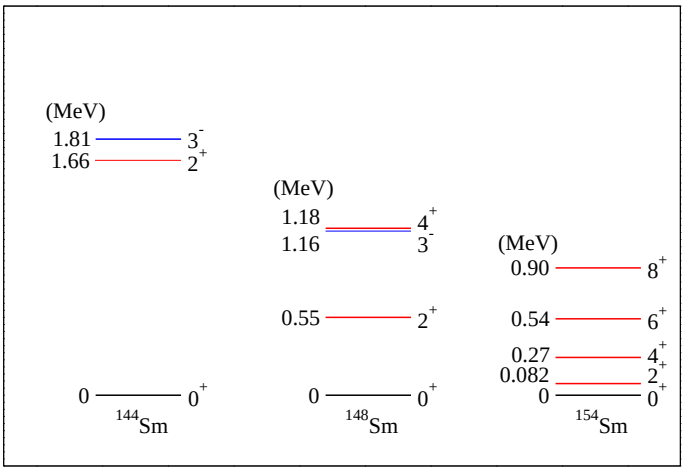

Fig. 4. Experimental low-lying spectra of ^{144,148,154}Sm nuclei.

§3. Coupled-channels formalism for heavy-ion fusion reactions

3.1. *Effects of nuclear structure on subbarrier fusion reactions*

The strong target dependence of subbarrier fusion cross sections shown in Fig. 3 suggests that the enhancement of fusion cross sections is due to low-lying collective excitations of the colliding nuclei during fusion. The low-lying excited states in even-even nuclei are collective states and strongly reflect the pairing correlation and shell structure. They are thus strongly coupled to the ground state and also have strong mass number and atomic number dependences. As an example, the low-lying spectra are shown in Fig. 4 for ^{144,148,154}Sm. The ^{144}Sm nucleus is close to the (sub-)shell closures (Z=64 and N = 82) and is characterized by a strong octupole vibration. ^{154}Sm, on the other hand, is a well-deformed nucleus and has a well-developed ground-state rotational band. ^{148}Sm is a transitional nucleus, and there exists a soft quadrupole vibration in the low-lying spectrum. One can clearly see that there is a strong correlation between the degree of enhancement of the fusion cross sections shown in Fig. 3 and, for example, the energy of the first 2^+ state.

In addition to the low-lying collective excitations, there are many other modes of excitation in atomic nuclei. Among them, noncollective excitations couple only weakly to the ground state and usually they do not significantly affect heavy-ion fusion reactions, even though the number of noncollective states is large.[57] Couplings to giant resonances are relatively strong owing to their collective character. However, since their excitation energies are relatively high and also are smooth functions of the mass number,[58)–60)] their effects can be effectively incorporated in the choice of internuclear potential through the adiabatic potential normalization (see the next section).

The effect of rotational excitations of a heavy deformed nucleus can be easily taken into account using the orientation average formula.[17),21),49),61)–63)] For an axially symmetric target nucleus, fusion cross sections are computed with this formula

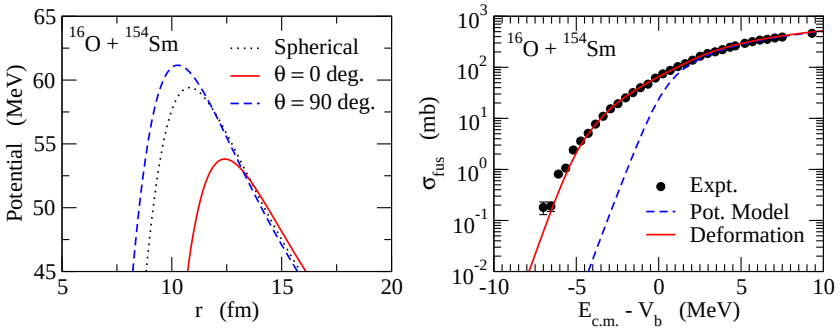

Fig. 5. (Left panel) Orientation dependence of fusion potential for the ^{16}O+^{154}Sm reaction. The solid and dashed lines are the potentials when the orientation of the deformed ^{154}Sm target is $\theta = 0$ and $\pi/2$, respectively. The dotted line denotes the potential when the deformation of ^{154}Sm is not taken into account. (Right panel) Fusion cross sections for the ^{16}O+^{154}Sm reaction. The dashed line is the result of the potential model calculation shown in Fig. 3, while the solid line is obtained by taking into account the deformation of the ^{154}Sm nucleus with Eq. (3·1). The experimental data are taken from Ref. 18).

as

$$\sigma_{\rm fus}(E) = \int_0^1 d(\cos\theta)\, \sigma_{\rm fus}(E;\theta), \tag{3·1}$$

where θ is the angle between the symmetry axis and the beam direction. $\sigma_{\rm fus}(E;\theta)$ is the fusion cross section for a *fixed* orientation angle, θ. This is obtained with, for example, a deformed Woods-Saxon potential,

$$V_N(r,\theta) = -\frac{V_0}{1+\exp[(r - R_0 - R_T\beta_2 Y_{20}(\theta) - R_T\beta_4 Y_{40}(\theta))/a]}, \tag{3·2}$$

which can be constructed by changing the target radius R_T in the Woods-Saxon potential, Eq. (2·4), to $R_T \to R_T(1+\beta_2 Y_{20}(\theta)+\beta_4 Y_{40}(\theta))$. See Ref. 64) for a recent application of this formula to the fusion of massive systems, in which the formula is combined with classical Langevin calculations.

The left panel of Fig. 5 shows the potential for the ^{16}O+^{154}Sm reaction obtained with the deformation parameters of $\beta_2 = 0.306$ and $\beta_4 = 0.05$. The deformation of the Coulomb potential is also taken into account (see §3.4 for details). The solid line shows the potential for $\theta = 0$. For this orientation angle, the potential is lowered by the deformation effect as compared with the spherical potential shown by the dotted line, because the attractive nuclear interaction is active from relatively large values of r. The opposite happens when $\theta = \pi/2$ as shown by the dashed line. The potential is distributed between the solid and dashed lines according to the value of the orientation angle, θ. The solid line in the right panel of Fig. 5 shows the fusion cross sections obtained by averaging the contributions of all the orientation angles through Eq. (3·1). Since the tunneling probability has an exponentially strong dependence on the barrier height, the fusion cross sections are significantly enhanced for the orientations that yield a lower barrier than the spherical case. It is remarkable that this simple calculation accounts well for the experimental enhancement of fusion

cross sections at subbarrier energies. Evidently, the effects of the nuclear structure significantly enhance fusion cross sections at energies below the Coulomb barrier, which makes fusion reactions an interesting probe for nuclear structures.

3.2. *Coupled-channels equations with full angular momentum coupling*

The effects of the nuclear structure can be taken into account in a more quantal way using the coupled-channels method. In order to formulate the coupled-channels method, consider a collision between two nuclei in the presence of the coupling of the relative motion, $\boldsymbol{r} = (r, \hat{\boldsymbol{r}})$, to a nuclear intrinsic motion ξ. We assume the following Hamiltonian for this system:

$$H(\boldsymbol{r}, \xi) = -\frac{\hbar^2}{2\mu}\nabla^2 + V(r) + H_0(\xi) + V_{\rm coup}(\boldsymbol{r}, \xi), \tag{3·3}$$

where $H_0(\xi)$ and $V_{\rm coup}(\boldsymbol{r}, \xi)$ are the intrinsic and coupling Hamiltonians, respectively. In general, the intrinsic degree of freedom ξ has a finite spin. We therefore expand the coupling Hamiltonian in multipoles as

$$V_{\rm coup}(\boldsymbol{r}, \xi) = \sum_{\lambda>0} f_\lambda(r) Y_\lambda(\hat{\boldsymbol{r}}) \cdot T_\lambda(\xi). \tag{3·4}$$

Here, $Y_\lambda(\hat{\boldsymbol{r}})$ are the spherical harmonics and $T_\lambda(\xi)$ are the spherical tensors constructed from the intrinsic coordinate. The dot indicates a scalar product. The sum is taken over all values of λ except for $\lambda = 0$, which is already included in the bare potential, $V(r)$.

For a given total angular momentum J and its z component M, one can define the channel wave functions as

$$\langle \hat{\boldsymbol{r}}\xi | (\alpha l I) JM \rangle = \sum_{m_l, m_I} \langle l m_l I m_I | JM \rangle Y_{l m_l}(\hat{\boldsymbol{r}}) \varphi_{\alpha I m_I}(\xi), \tag{3·5}$$

where l and I are the orbital and intrinsic angular momenta, respectively. $\varphi_{\alpha I m_I}(\xi)$ are the wave functions of the intrinsic motion, which obey

$$H_0(\xi)\varphi_{\alpha I m_I}(\xi) = \epsilon_{\alpha I}\, \varphi_{\alpha I m_I}(\xi). \tag{3·6}$$

Here, α denotes any quantum number apart from the angular momentum. Expanding the total wave function with the channel wave functions as

$$\Psi_J(\boldsymbol{r}, \xi) = \sum_{\alpha, l, I} \frac{u^J_{\alpha l I}(r)}{r} \langle \hat{\boldsymbol{r}}\xi | (\alpha l I) JM \rangle, \tag{3·7}$$

the coupled-channels equations for $u^J_{\alpha l I}(r)$ are obtained as

$$\left[-\frac{\hbar^2}{2\mu}\frac{d^2}{dr^2} + \frac{l(l+1)\hbar^2}{2\mu r^2} + V(r) - E + \epsilon_{\alpha I} \right] u^J_{\alpha l I}(r) + \sum_{\alpha', l', I'} V^J_{\alpha l I; \alpha' l' I'}(r) u^J_{\alpha' l' I'}(r) = 0, \tag{3·8}$$

where the coupling matrix elements $V^J_{\alpha lI;\alpha' l' I'}(r)$ are given as[65]

$$V^J_{\alpha lI;\alpha' l' I'}(r) = \langle (\alpha lI) JM | V_{\rm coup}(\boldsymbol{r},\xi) | (\alpha' l' I') JM \rangle, \tag{3·9}$$

$$= \sum_\lambda (-)^{l'+I+J} f_\lambda(r) \langle l || Y_\lambda || l' \rangle \langle \alpha I || T_\lambda || \alpha' I' \rangle \times \left\{ \begin{array}{ccc} J & I & l \\ \lambda & l' & I' \end{array} \right\}. \tag{3·10}$$

Note that these matrix elements are independent of M.

For the sake of simplicity of notation, in the following let us introduce a simplified notation, $n = \{\alpha, l, I\}$, and suppress the index J. The coupled-channels equation (3·8) then becomes,

$$\left[-\frac{\hbar^2}{2\mu}\frac{d^2}{dr^2} + \frac{l_n(l_n+1)\hbar^2}{2\mu r^2} + V(r) - E + \epsilon_n \right] u_n(r) + \sum_{n'} V_{nn'}(r) u_{n'}(r) = 0. \tag{3·11}$$

These coupled-channels equations are solved with the IWBC of

$$u_n(r) \sim \sqrt{\frac{k_{n_i}}{k_n(r)}}\, \mathcal{T}^J_{nn_i} \exp\left(-i \int_{r_{\rm abs}}^r k_n(r') dr' \right), \qquad r \le r_{\rm abs} \tag{3·12}$$

$$= H^{(-)}_{l_n}(k_n r)\delta_{n,n_i} - \sqrt{\frac{k_{n_i}}{k_n}}\, \mathcal{S}^J_{nn_i} H^{(+)}_{l_n}(k_n r), \qquad r \to \infty \tag{3·13}$$

where n_i denotes the entrance channel. The local wave number $k_n(r)$ is defined by

$$k_n(r) = \sqrt{\frac{2\mu}{\hbar^2}\left(E - \epsilon_n - \frac{l_n(l_n+1)\hbar^2}{2\mu r^2} - V(r) \right)}, \tag{3·14}$$

whereas $k_n = k_n(r=\infty) = \sqrt{2\mu(E-\epsilon_n)/\hbar^2}$. Once the transmission coefficients $\mathcal{T}^J_{nn_i}$ are obtained, the inclusive penetrability of the Coulomb potential barrier is given by

$$P_J(E) = \sum_n |\mathcal{T}^J_{nn_i}|^2. \tag{3·15}$$

The fusion cross section is then given by

$$\sigma_{\rm fus}(E) = \frac{\pi}{k^2} \sum_J (2J+1) P_J(E), \tag{3·16}$$

where we have assumed that the initial intrinsic state has spin zero, $I_i = 0$. This equation for the fusion cross section is similar to Eq. (2·17) except that the penetrability $P_J(E)$ is now influenced by the effects of channel coupling.

3.3. *Iso-centrifugal approximation*

The full coupled-channels calculations (3·11) quickly become intricate if many physical channels are included. The dimension of the resulting coupled-channels

problem is in general too large for practical purposes. For this reason, the iso-centrifugal approximation, which is sometimes referred to as the no-Coriolis approximation or the rotating frame approximation, has often been used.[21),48),63),66)–70)] In the iso-centrifugal approximation to the coupled-channels equations, Eq. (3·11), one first replaces the angular momentum of the relative motion in each channel by the total angular momentum J, that is,

$$\frac{l_n(l_n+1)\hbar^2}{2\mu r^2} \approx \frac{J(J+1)\hbar^2}{2\mu r^2}. \tag{3·17}$$

This corresponds to assuming that the change in the orbital angular momentum due to the excitation of the intrinsic degree of freedom is negligible. Introducing the weighted average wave function

$$\bar{u}_I(r) = (-)^I \sum_l \langle J0I0|l0\rangle u_{lI}(r), \tag{3·18}$$

where we have suppressed the index α for simplicity, and using the relation

$$\begin{aligned}&\sum_l (-)^{l'+J+\lambda}\sqrt{2l+1}\left\{\begin{array}{ccc} J & I & l \\ \lambda & l' & I' \end{array}\right\}\langle l0\lambda0|l'0\rangle\langle J0I0|l0\rangle \\ &= \frac{(-)^{I'}}{\sqrt{2I+1}}\langle J0I'0|l'0\rangle\langle I'0\lambda0|I0\rangle,\end{aligned} \tag{3·19}$$

one finds that the wave function $\bar{u}_I(r)$ obeys the reduced coupled-channels equations

$$\begin{aligned}&\left(-\frac{\hbar^2}{2\mu}\frac{d^2}{dr^2} + \frac{J(J+1)\hbar^2}{2\mu r^2} + V(r) - E + \epsilon_I\right)\bar{u}_I(r) \\ &+ \sum_{I'}\sum_{\lambda}\sqrt{\frac{2\lambda+1}{4\pi}} f_\lambda(r)\langle\varphi_{I0}|T_{\lambda0}|\varphi_{I'0}\rangle\bar{u}_{I'}(r) = 0.\end{aligned} \tag{3·20}$$

These are simply the coupled-channels equations for a spin-zero system with the interaction Hamiltonian given by

$$V_{\rm coup} = \sum_\lambda f_\lambda(r) Y_\lambda(\hat{\boldsymbol{r}}=0)\cdot T_\lambda = \sum_\lambda \sqrt{\frac{2\lambda+1}{4\pi}} f_\lambda(r) T_{\lambda0}. \tag{3·21}$$

In solving the reduced coupled-channels equations, similar boundary conditions are imposed for $\bar{u}_I$ as those for u_{lI},

$$\bar{u}_I(r) \sim \sqrt{\frac{k_{I_i}}{k_I(r)}}\,\bar{\mathcal{T}}^J_{II_i}\exp\left(-i\int_{r_{\rm abs}}^r k_I(r')dr'\right), \qquad r \le r_{\rm abs}, \tag{3·22}$$

$$= H_J^{(-)}(k_I r)\delta_{I,I_i} - \sqrt{\frac{k_{I_i}}{k_I}}\,\bar{S}^J_{II_i} H_J^{(+)}(k_I r), \qquad r\to\infty, \tag{3·23}$$

where k_I and $k_I(r)$ are defined in the same way as in Eq. (3·14). The fusion cross section is then given by Eq. (3·16) with the penetrability of

$$P_J(E) = \sum_I |\bar{\mathcal{T}}^J_{II_i}|^2. \tag{3·24}$$

Since the reduced coupled-channels equations in the iso-centrifugal approximation are equivalent to the coupled-channels equations with a spin-zero intrinsic motion, the complicated angular momentum couplings disappear. A remarkable fact is that the dimension of the coupled-channels equations is drastically reduced in this approximation. For example, if one includes four intrinsic states with 2^+, 4^+, 6^+, and 8^+ together with the ground state in the coupled-channels equations, the original equations have 25 dimensions for $J \geq 8$, while the dimension is reduced to 5 in the iso-centrifugal approximation. The validity of the iso-centrifugal approximation has been well tested for heavy-ion fusion reactions, and it has been concluded that the iso-centrifugal approximation leads to negligible errors in calculating fusion cross sections.[63),67)]

3.4. *Coupling to low-lying collective states*

3.4.1. Vibrational coupling

Let us now discuss the explicit form of the coupling Hamiltonian $V_{\rm coup}$ for heavy-ion fusion reactions. We first consider couplings of the relative motion to the 2^λ-pole surface vibration of a target nucleus. In the geometrical model of Bohr and Mottelson, the radius of the vibrating target is parameterized as

$$R(\theta,\phi) = R_T\left(1+\sum_\mu \alpha_{\lambda\mu} Y^*_{\lambda\mu}(\theta,\phi)\right), \tag{3·25}$$

where R_T is the equivalent sharp surface radius and $\alpha_{\lambda\mu}$ is the surface coordinate of the target nucleus. To the lowest order, the surface oscillation is approximated by a harmonic oscillator, and the Hamiltonian for the intrinsic motion is given by

$$H_0 = \hbar\omega_\lambda\left(\sum_\mu a^\dagger_{\lambda\mu}a_{\lambda\mu} + \frac{2\lambda+1}{2}\right). \tag{3·26}$$

Here, $\hbar\omega_\lambda$ are the oscillator quanta and $a^\dagger_{\lambda\mu}$ and $a_{\lambda\mu}$ are the phonon creation and annihilation operators, respectively. The surface coordinate $\alpha_{\lambda\mu}$ is related to the phonon creation and annihilation operators by

$$\alpha_{\lambda\mu} = \alpha_0\left(a^\dagger_{\lambda\mu} + (-)^\mu a_{\lambda\mu}\right) = \frac{\beta_\lambda}{\sqrt{2\lambda+1}}\left(a^\dagger_{\lambda\mu} + (-)^\mu a_{\lambda\mu}\right), \tag{3·27}$$

where $\alpha_0 = \beta_\lambda/\sqrt{2\lambda+1}$ is the amplitude of the zero-point motion.[58)] The deformation parameter β_λ can be estimated from the experimental transition probability using (see Eq. (3·34) below)

$$\beta_\lambda = \frac{4\pi}{3Z_T R_T^\lambda}\sqrt{\frac{B(E\lambda)\uparrow}{e^2}}. \tag{3·28}$$

The surface vibration of the target nucleus modifies both the nuclear and Coulomb interactions between the colliding nuclei. In the collective model, the nuclear interaction is assumed to be a function of the separation distance between the vibrating

surfaces of the colliding nuclei, and is thus given as

$$V^{(N)}(\boldsymbol{r}, \alpha_{\lambda\mu}) = V_N\left(r - R_T \sum_{\mu} \alpha_{\lambda\mu} Y^*_{\lambda\mu}(\hat{\boldsymbol{r}})\right). \tag{3·29}$$

If the amplitude of the zero-point motion of the vibration is small, one can expand this equation in terms of $\alpha_{\lambda\mu}$ and keep only the linear term,

$$V^{(N)}(\boldsymbol{r}, \alpha_{\lambda\mu}) = V_N(r) - R_T \frac{dV_N(r)}{dr} \sum_{\mu} \alpha_{\lambda\mu} Y^*_{\lambda\mu}(\hat{\boldsymbol{r}}). \tag{3·30}$$

This approximation is called the linear coupling approximation. The first term of the right-hand side (r.h.s.) of Eq. (3·30) is the bare nuclear potential in the absence of the coupling, while the second term is the nuclear component of the coupling Hamiltonian. Even though the linear coupling approximation does not work well for heavy-ion fusion reactions,[48),71)] we employ it in this subsection in order to illustrate the coupling scheme. In §3.5, we will discuss how the higher order terms can be taken into account in the coupling matrix.

The Coulomb component of the coupling Hamiltonian is evaluated as follows. The Coulomb potential between the spherical projectile and the vibrating target is given by

$$V_C(\boldsymbol{r}) = \int d\boldsymbol{r}' \frac{Z_P Z_T e^2}{|\boldsymbol{r} - \boldsymbol{r}'|} \rho_T(\boldsymbol{r}') = \frac{Z_P Z_T e^2}{r} + \sum_{\lambda' \neq 0} \sum_{\mu'} \frac{4\pi Z_P e}{2\lambda' + 1} Q_{\lambda'\mu'} Y^*_{\lambda'\mu'}(\hat{\boldsymbol{r}}) \frac{1}{r^{\lambda'+1}}, \tag{3·31}$$

where ρ_T is the charge density of the target nucleus and $Q_{\lambda'\mu'}$ is the electric multipole operator, defined by

$$Q_{\lambda'\mu'} = \int d\boldsymbol{r} Z_T e \rho_T(\boldsymbol{r}) r^{\lambda'} Y_{\lambda'\mu'}(\hat{\boldsymbol{r}}). \tag{3·32}$$

The first term of the r.h.s. of Eq. (3·31) is the bare Coulomb interaction, and the second term is the Coulomb component of the coupling Hamiltonian. In obtaining Eq. (3·31), we have used the formula

$$\frac{1}{|\boldsymbol{r} - \boldsymbol{r}'|} = \sum_{\lambda'\mu'} \frac{4\pi}{2\lambda' + 1} \frac{r_<^{\lambda'}}{r_>^{\lambda'+1}} Y_{\lambda'\mu'}(\hat{\boldsymbol{r}}') Y^*_{\lambda'\mu'}(\hat{\boldsymbol{r}}), \tag{3·33}$$

and have assumed that the relative coordinate r is larger than the charge radius of the target nucleus. If we assume a sharp matter distribution for the target nucleus, the electric multipole operator is given by

$$Q_{\lambda'\mu'} = \frac{3e}{4\pi} Z_T R_T^{\lambda} \alpha_{\lambda\mu} \delta_{\lambda\mu,\lambda'\mu'}, \tag{3·34}$$

up to the first order of the surface coordinate $\alpha_{\lambda\mu}$.

By combining Eqs. (3·30), (3·31), and (3·34), the coupling Hamiltonian is expressed by

$$V_{\rm coup}(\boldsymbol{r},\alpha_\lambda) = f_\lambda(r)\sum_\mu \alpha_{\lambda\mu}Y^*_{\lambda\mu}(\hat{\boldsymbol{r}}), \tag{3·35}$$

up to the first order of $\alpha_{\lambda\mu}$. Here, $f_\lambda(r)$ is the coupling form factor, given by

$$f_\lambda(r) = -R_T\frac{dV_N}{dr} + \frac{3}{2\lambda+1}Z_PZ_Te^2\frac{R_T^\lambda}{r^{\lambda+1}}, \tag{3·36}$$

where the first and second terms are the nuclear and Coulomb coupling form factors, respectively. Transforming to the rotating frame, the coupling Hamiltonian used in the iso-centrifugal approximation is then given by (see Eq. (3·21))

$$V_{\rm coup}(r,\alpha_{\lambda 0}) = \sqrt{\frac{2\lambda+1}{4\pi}}f_\lambda(r)\alpha_{\lambda 0} = \frac{\beta_\lambda}{\sqrt{4\pi}}f_\lambda(r)\left(a^\dagger_{\lambda 0}+a_{\lambda 0}\right). \tag{3·37}$$

Note that the coupling form factor f_λ has the value

$$f_\lambda(R_b) = \frac{Z_PZ_Te^2}{R_b}\left(\frac{3}{2\lambda+1}\frac{R_T^\lambda}{R_b^\lambda} - \frac{R_T}{R_b}\right) \tag{3·38}$$

at the position of the bare Coulomb barrier, R_b, and the coupling strength is approximately proportional to the charge product of the colliding nuclei.

In the previous subsection, we showed that the iso-centrifugal approximation drastically reduces the dimension of the coupled-channels equations. A further reduction can be achieved by introducing effective multiphonon channels.[66),69)] In general, the multiphonon states of the vibrator have several levels, which are distinguished from each other by the angular momentum and the seniority.[58)] For example, for the quadrupole surface vibrations, the two-phonon state has three levels $(0^+, 2^+, 4^+)$, which are degenerate in energy in the harmonic limit. The one-phonon state, $|2^+_1\rangle = a^\dagger_{20}|0\rangle$, couples only to a particular combination of these triplet states,

$$|2\rangle = \sum_{I=0,2,4}\langle 2020|I0\rangle|I0\rangle = \frac{1}{\sqrt{2!}}(a^\dagger_{20})^2|0\rangle. \tag{3·39}$$

It is thus sufficient to include this single state in the calculations, instead of three triplet states. In the same way, one can introduce the n-phonon channel for a multipolarity λ as

$$|n\rangle = \frac{1}{\sqrt{n!}}(a^\dagger_{\lambda 0})^n|0\rangle. \tag{3·40}$$

See Appendix C for the case of two different vibrational modes of excitation (e.g., quadrupole and octupole vibrations).

If one truncates the phonon space up to the two-phonon state, the corresponding coupling matrix is then given by

$$H_0 + V_{\rm coup} = \begin{pmatrix} 0 & F(r) & 0 \\ F(r) & \hbar\omega_\lambda & \sqrt{2}F(r) \\ 0 & \sqrt{2}F(r) & 2\hbar\omega_\lambda \end{pmatrix}, \tag{3·41}$$

where $F(r)$ is defined as $\beta_\lambda f_\lambda(r)/\sqrt{4\pi}$.

The effects of deviations from the harmonic oscillator limit presented in this subsection on subbarrier fusion reactions have been discussed in Refs. 72) and 73).

3.4.2. Rotational coupling

We next consider couplings to the ground rotational band of a deformed target. To this end, it is convenient to transform to the body-fixed frame so that the z axis is along the orientation of the deformed target. The surface coordinate $\alpha_{\lambda\mu}$ is then transformed to

$$a_{\lambda\mu} = \sum_{\mu'} D^{\lambda}_{\mu'\mu}(\phi_d, \theta_d, \chi_d)\alpha_{\lambda\mu'}, \tag{3·42}$$

where ϕ_d, θ_d, and χ_d are the Euler angles which specify the body-fixed frame, and thus the orientation of the target. If we are particularly interested in the quadrupole deformation (λ=2), the surface coordinates in the body-fixed frame are expressed as

$$a_{20} = \beta_2 \cos\gamma, \tag{3·43}$$

$$a_{22} = a_{2-2} = \frac{1}{\sqrt{2}}\beta_2 \sin\gamma, \tag{3·44}$$

$$a_{21} = a_{2-1} = 0. \tag{3·45}$$

If we further assume that the deformation is axial symmetric (i.e., $\gamma = 0$), the coupling Hamiltonian for the rotational coupling is (see Eq. (3·35))

$$V_{\rm coup}(\boldsymbol{r}, \theta_d, \phi_d) = f_2(r) \sum_{\mu} \beta_2 \sqrt{\frac{4\pi}{5}} Y_{2\mu}(\theta_d, \phi_d) Y^*_{2\mu}(\hat{\boldsymbol{r}}). \tag{3·46}$$

In order to obtain this equation, we have used the relation

$$D^L_{M0}(\phi, \theta, \chi) = \sqrt{\frac{4\pi}{2L+1}} Y^*_{LM}(\theta, \phi). \tag{3·47}$$

The coupling Hamiltonian in the rotating frame is thus given by

$$V_{\rm coup}(r, \theta) = f_2(r)\beta_2 Y_{20}(\theta), \tag{3·48}$$

where θ is the angle between (θ_d, ϕ_d) and $\hat{\boldsymbol{r}}$, that is, the direction of the orientation of the target measured from the direction of the relative motion between the colliding nuclei. Since the wave function for the $|I0\rangle$ state in the ground rotational band is given by $|I0\rangle = |Y_{I0}\rangle$, the corresponding coupling matrix is given by

$$H_0 + V_{\rm coup} = H_0 + f_2(r)\beta_2 \langle Y_{I'0}|Y_{20}|Y_{I0}\rangle = \begin{pmatrix} 0 & F(r) & 0 \\ F(r) & \epsilon_2 + \frac{2\sqrt{5}}{7}F(r) & \frac{6}{7}F(r) \\ 0 & \frac{6}{7}F(r) & \frac{10}{3}\epsilon_2 + \frac{20\sqrt{5}}{77}F(r) \end{pmatrix} \tag{3·49}$$

when the rotational band is truncated at the first 4^+ state. Here, ϵ_2 is the excitation energy of the first 2^+ state and $F(r)$ is defined as $\beta_2 f_2(r)/\sqrt{4\pi}$ as in Eq. (3·41).

One of the main differences between the vibrational (3·41) and rotational (3·49) couplings is that the latter has a diagonal component that is proportional to the deformation parameter β_2. The diagonal component in the rotational coupling is referred to as the *reorientation effect* and has been used in the Coulomb excitation technique to determine the sign of the deformation parameter.[74] Note that the results of the coupled-channels calculations are independent of the sign of β_2 for the vibrational coupling.

The effects of the γ deformation on subbarrier fusion were studied in Ref. 75). If there is a finite γ deformation, the coupling Hamiltonian in the rotating frame becomes

$$V_{\rm coup}(r,\theta,\phi) = f_2(r)\left(\beta_2\cos\gamma Y_{20}(\theta) + \frac{1}{\sqrt{2}}\beta_2\sin\gamma\left(Y_{22}(\theta,\phi)+Y_{2-2}(\theta,\phi)\right)\right). \tag{3·50}$$

Higher order deformations can also be taken into account in a similar way as the quadrupole deformation. For example, if there is an axial symmetric hexadecapole deformation in addition to a quadrupole deformation, the coupling Hamiltonian becomes

$$V_{\rm coup}(r,\theta) = f_2(r)\beta_2 Y_{20}(\theta) + f_4(r)\beta_4 Y_{40}(\theta), \tag{3·51}$$

where β_4 is the hexadecapole deformation parameter.

3.5. *All order couplings*

In the previous subsection, for simplicity, we have used the linear coupling approximation and expanded the coupling Hamiltonian in terms of the deformation parameter. However, it has been shown that the higher order terms play an important role in heavy-ion subbarrier fusion reactions.[48),71),76)–79)] These higher order terms can be evaluated as follows.[48)] If we employ the Woods-Saxon potential, Eq. (2·4), the nuclear coupling Hamiltonian can be generated by changing the target radius in the potential to a dynamical operator,

$$R_0 \to R_0 + \hat{O}, \tag{3·52}$$

that is,

$$V_N(r) \to V_N(r,\hat{O}) = -\frac{V_0}{1+\exp((r-R_0-\hat{O})/a)}. \tag{3·53}$$

For the vibrational coupling, the operator $\hat{O}$ is given by (see Eq. (3·37))

$$\hat{O} = \frac{\beta_\lambda}{\sqrt{4\pi}}R_T(a^\dagger_{\lambda 0} + a_{\lambda 0}), \tag{3·54}$$

while for the rotational coupling it is given by (see Eqs. (3·2) and (3·48))

$$\hat{O} = \beta_2 R_T Y_{20}(\theta) + \beta_4 R_T Y_{40}(\theta). \tag{3·55}$$

The matrix elements of the coupling Hamiltonian can be easily obtained using matrix algebra.[80)] In this algebra, one first looks for the eigenvalues and eigenvectors of the operator $\hat{O}$ which satisfy

$$\hat{O}|\alpha\rangle = \lambda_\alpha|\alpha\rangle. \tag{3·56}$$

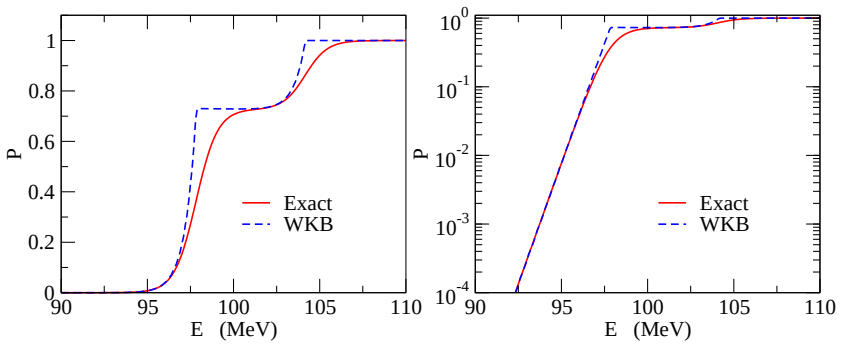

Fig. 6. Barrier penetrability for a two-level problem as a function of energy E in linear (left panel) and logarithmic (right panel) scales. The solid and dashed lines are the exact solution and the WKB approximation, respectively.

This is done by numerically diagonalizing the matrix $\hat{O}$, whose elements are given by

$$\hat{O}_{nm} = \frac{\beta_\lambda}{\sqrt{4\pi}} R_T(\sqrt{m}\delta_{n,m-1} + \sqrt{n}\delta_{n,m+1}) \tag{3·57}$$

for the vibrational case and

$$\begin{aligned}\hat{O}_{II'} = &\sqrt{\frac{5(2I+1)(2I'+1)}{4\pi}}\beta_2 R_T \begin{pmatrix} I & 2 & I' \\ 0 & 0 & 0 \end{pmatrix}^2 \\ &+\sqrt{\frac{9(2I+1)(2I'+1)}{4\pi}}\beta_4 R_T \begin{pmatrix} I & 4 & I' \\ 0 & 0 & 0 \end{pmatrix}^2 \end{aligned} \tag{3·58}$$

for the rotational case. The nuclear coupling matrix elements are then evaluated as

$$\begin{aligned} V_{nm}^{(N)} &= \langle n|V_N(r,\hat{O})|m\rangle - V_N(r)\delta_{n,m}, \\ &= \sum_\alpha \langle n|\alpha\rangle\langle\alpha|m\rangle V_N(r,\lambda_\alpha) - V_N(r)\delta_{n,m}. \end{aligned} \tag{3·59}$$

The last term in this equation is included to avoid the double counting of the diagonal component.

The computer code `CCFULL` has been written with this scheme,[48] and has been used in analyzing recent experimental fusion cross sections for many systems. `CCFULL` also includes the second-order terms in the Coulomb coupling for the rotational case, while it uses the linear coupling approximation for the Coulomb coupling in the vibrational case.[48]

3.6. *WKB approximation for multichannel penetrability*

Whereas the coupled-channels equations, Eq. (3·20), can be numerically solved, for example, with the computer code `CCFULL` once the coupling Hamiltonian has been set up, it is always useful to have an approximate solution. In the next section, we will discuss the limit of the zero excitation energy for intrinsic degrees of freedom, in which the coupled-channels equations are decoupled. In this subsection, on

the other hand, we discuss another approximate solution based on the semiclassical approximation.

The penetrability in the Wentzel, Kramers, and Brillouin (WKB) approximation is well known for a one dimensional potential $V(x)$ and is given by

$$P(E) = \exp\left[-2\int_{x_0}^{x_1} dx' \sqrt{\frac{2\mu}{\hbar^2}(V(x') - E)}\right], \tag{3·60}$$

where x_0 and x_1 are the inner and outer turning points satisfying $V(x_0) = V(x_1) = E$, respectively. One can also introduce the uniform approximation to take into account the multiple reflection under the barrier and obtain a formula that is valid at all energies from below to above the barrier,[81)–85)]

$$P(E) = \frac{1}{1 + \exp\left[2\int_{x_0}^{x_1} dx' \sqrt{\frac{2\mu}{\hbar^2}(V(x') - E)}\right]}. \tag{3·61}$$

It has been shown in Ref. 86) that one can generalize the primitive WKB formula (3·60) to a multichannel problem as

$$P = \sum_n \left| \left\langle n \left| \prod_i e^{i\boldsymbol{q}(x_i)\Delta x} \right| n_i \right\rangle \right|^2, \tag{3·62}$$

where $\boldsymbol{q}(x) = [2\mu(E - \boldsymbol{W}(x))/\hbar^2]^{1/2}$ with $W_{nm}(x) = \langle n|V(x) + H_0(\xi) + V_{\rm coup}(x,\xi)|m\rangle$ (see Eq. (3·3)). Here, we have discretized the coordinate x with a mesh spacing of Δx. For a single-channel problem, Eq. (3·62) is reduced to Eq. (3·60).

Figure 6 shows the result of the multichannel WKB approximation for a two-level problem given by

$$\boldsymbol{W}(x) = \begin{pmatrix} V(x) & F(x) \\ F(x) & V(x) + \epsilon \end{pmatrix} = V(x)\begin{pmatrix} 1 & 0 \\ 0 & 1 \end{pmatrix} + F(x)\begin{pmatrix} 0 & 1 \\ 1 & 0 \end{pmatrix} + \begin{pmatrix} 0 & 0 \\ 0 & \epsilon \end{pmatrix}, \tag{3·63}$$

with

$$V(x) = V_0 e^{-x^2/2s^2}, \qquad F(x) = F_0 e^{-x^2/2s_f^2}. \tag{3·64}$$

The parameters are chosen following Ref. 19) to be V_0=100 MeV, F_0=3 MeV, and $s = s_f$ =3 fm, which mimic the fusion reaction between two ^{58}Ni nuclei. The excitation energy ϵ and the mass μ are taken to be 2 MeV and $29m_N$, respectively, where m_N is the nucleon mass. It is remarkable that the WKB formula (3·62) reproduces almost perfectly the exact solution at energies well below the barrier. The WKB formula breaks down at energies around the barrier, as in the single-channel problem.

The figure also suggests that the penetrability is given by a weighted sum of two penetrabilities,

$$P(E) = w_1 P(E; \lambda_1(x)) + w_2 P(E; \lambda_2(x)), \tag{3·65}$$

where $\lambda_i(x)$ are the eigen-potentials, $\lambda_i(x) = V(x) + [\epsilon \pm \sqrt{\epsilon^2 + 4F(x)^2}]/2$, obtained by diagonalizing the matrix $\boldsymbol{W}(x)$ given by Eq. (3·63). We will discuss this point in the next section.

§4. Barrier distribution representation of multichannel penetrability

4.1. *Sudden tunneling limit and barrier distribution*

In the limit of vanishing excitation energy for the intrinsic motion (i.e., in the limit of $\epsilon_I \to 0$), the reduced coupled-channels equations (3·20) are completely decoupled. This limit corresponds to the case where the tunneling occurs much faster than the intrinsic motion, and is thus referred to as the sudden tunneling limit. In this limit, the coupling matrix, defined as

$$V_{II'} \equiv \epsilon_I \delta_{I,I'} + \sqrt{\frac{2\lambda+1}{4\pi}} f_\lambda(r) \langle \varphi_{I0} | T_{\lambda 0} | \varphi_{I'0} \rangle, \tag{4·1}$$

can be diagonalized independently of r (for simplicity we consider only a single value of λ). See also Eq. (3·63). It is then easy to prove that the fusion cross section is given as a weighted sum of the cross sections for uncoupled eigenchannels,[21),87)]

$$\sigma_{\rm fus}(E) = \sum_\alpha w_\alpha \, \sigma_{\rm fus}^{(\alpha)}(E), \tag{4·2}$$

where $\sigma_{\rm fus}^{(\alpha)}(E)$ is the fusion cross section for a potential in the eigenchannel α, i.e., $V_\alpha(r) = V(r) + \lambda_\alpha(r)$. The same relation also holds for quasi-elastic scattering.[63),87),88)] Here, $\lambda_\alpha(r)$ is the eigenvalue of the coupling matrix (4·1) (when ϵ_I is zero, $\lambda_\alpha(r)$ is simply given by $\lambda_\alpha \cdot f_\lambda(r)$). The weight factor w_α is given by $w_\alpha = |U_{0\alpha}|^2$, where U is the unitary matrix which diagonalizes Eq. (4·1). Note that the unitarity of the matrix U leads to the relation that the sum of all the weight factors, $\sum_\alpha w_\alpha$, is unity.[21)]

The resultant formula (4·2) in the sudden tunneling limit can be interpreted in the following way. In the absence of coupling, the incident particle encounters only the single potential barrier, $V(r)$. When coupling occurs, the bare potential splits into many barriers. Some of them are lower than the bare potential and some of them higher. In this picture, the potential barriers are distributed with appropriate weight factors, w_α.

The orientation average formula discussed in §3.1 (see Eq. (3·1)) for a deformed target nucleus can also be obtained from the coupled-channels equations by taking the sudden tunneling limit.[21)] To show this, first note that the coupling Hamiltonian is diagonal with respect to the orientation angle, θ. If all the members of the rotational band are included in the coupled-channels equations, the eigenstates of the coupling Hamiltonian matrix then become the same as the angle vector $|\theta\rangle$ with the eigenvalue given by the deformed Woods-Saxon potential, Eq. (3·2).[21),89),90)] The weight factor in this case is simply given by $w(\theta) = |\langle \theta | \varphi_{I=0} \rangle|^2 = |Y_{00}(\theta)|^2$.

The physical interpretation of the orientation average formula is that the fusion reaction takes place so suddenly that the orientation angle is fixed during the fusion reaction. This is justified because the first 2^+ state of a heavy deformed nucleus is small (see Fig. 4), corresponding to a large moment of inertia for the rotational motion. As the orientation angles are distributed according to the wave function for the ground state, the fusion cross section can be computed by first fixing the

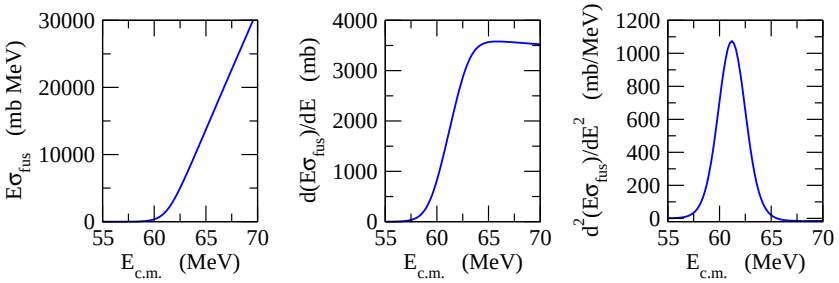

Fig. 7. Product of energy E and fusion cross section $\sigma_{\rm fus}$, $E\sigma_{\rm fus}$, for the ^{16}O+^{144}Sm reaction obtained with the potential model (left panel). The middle and right panels show the first and second energy derivatives of $E\sigma_{\rm fus}$, respectively.

orientation angle and then averaging over the orientation angle with the appropriate weight factor, $w(\theta)$. The applicability of this formula has been investigated in Ref. 62) in the reactions of a ^{154}Sm target with various projectiles ranging from ^{12}C to ^{40}Ar. It has been shown that the formula works well, although the agreement with the exact coupled-channels calculations, which take into account the finite excitation energy of the rotational excitation, becomes slightly worse for a large value of the charge product of the projectile and the target nuclei.

4.2. *Fusion barrier distribution*

Rowley et al. have proposed a method to directly extract how the barriers are distributed from the experimental fusion cross sections.[13),22)] In order to illustrate the method, let us first discuss the classical fusion cross section given by

$$\sigma_{\rm fus}^{cl}(E) = \pi R_b^2 \left(1 - \frac{V_b}{E}\right) \theta(E - V_b). \tag{4·3}$$

From this expression, it is clear that the first derivative of $E\sigma_{\rm fus}^{cl}$ is proportional to the classical penetrability for a one-dimensional barrier of height V_b,

$$\frac{d}{dE}[E\sigma_{\rm fus}^{cl}(E)] = \pi R_b^2\, \theta(E - V_b) = \pi R_b^2\, P_{cl}(E), \tag{4·4}$$

and that the second derivative is proportional to a delta function,

$$\frac{d^2}{dE^2}[E\sigma_{\rm fus}^{cl}(E)] = \pi R_b^2\, \delta(E - V_b). \tag{4·5}$$

In quantum mechanics, the tunneling effect smears the delta function in Eq. (4·5). As we have noted in §2.2, an analytic formula for the fusion cross section can be obtained if one approximates the Coulomb barrier by an inverse parabola, see Eq. (B·5) in Appendix B. Again, the first derivative of $E\sigma_{\rm fus}$ is proportional to the s-wave penetrability for a parabolic barrier,

$$\frac{d}{dE}[E\sigma_{\rm fus}(E)] = \pi R_b^2 \frac{1}{1 + \exp\left[-\frac{2\pi}{\hbar\Omega}(E - V_b)\right]} = \pi R_b^2\, P(E), \tag{4·6}$$

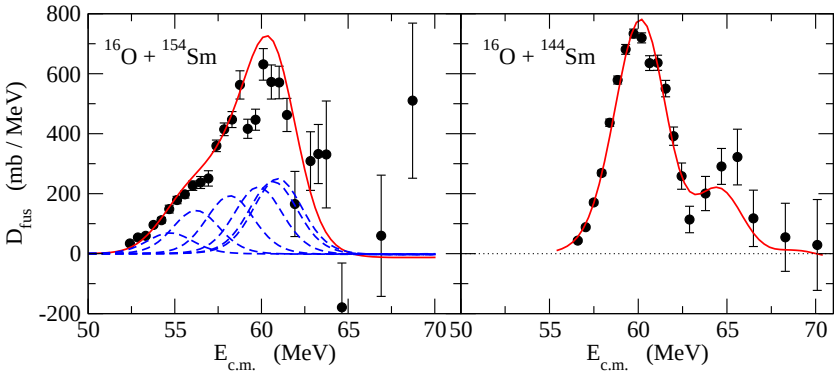

Fig. 8. (Left panel) Fusion barrier distribution $D_{\rm fus}(E) = d^2(E\sigma_{\rm fus})/dE^2$ for the ^{16}O+^{154}Sm reaction.[18] The solid line is obtained with the orientation average formula, which corresponds to the solid line in Fig. 5. The dashed lines indicate the contributions from six individual eigenbarriers (i.e., orientation angles). (Right panel) Fusion barrier distribution for the ^{16}O+^{144}Sm reaction.[18] The solid line shows the result of the coupled-channels calculations, which take into account the anharmonic double-phonon excitations of ^{144}Sm.[72),73)]

and the second derivative is proportional to the derivative of the s-wave penetrability,

$$\frac{d^2}{dE^2}[E\sigma_{\rm fus}(E)] = \pi R_b^2 \frac{2\pi}{\hbar\Omega} \frac{e^x}{(1+e^x)^2} = \pi R_b^2 \frac{dP(E)}{dE}, \tag{4·7}$$

where $x = -2\pi(E - V_b)/\hbar\Omega$. As shown in Fig. 7, this function has the following properties: i) it is symmetric around $E = V_b$, ii) it is centered at $E = V_b$, iii) its integral over E is πR_b^2, and iv) it has a relatively narrow width of around $\ln(3 + \sqrt{8})\hbar\Omega/\pi \sim 0.56\hbar\Omega$.

In the presence of channel couplings, Eq. (4·2) immediately leads to

$$D_{\rm fus} = \frac{d^2}{dE^2}[E\sigma_{\rm fus}(E)] = \sum_\alpha w_\alpha \frac{d^2}{dE^2}[E\sigma_{\rm fus}^{(\alpha)}(E)]. \tag{4·8}$$

This function has been referred to as the fusion barrier distribution. As an example, the left panel of Fig. 8 shows the barrier distribution for the ^{16}O+^{154}Sm reaction, whose fusion cross sections have already been shown in Fig. 5. We replace the integral in Eq. (3·1) with the $(I_{\rm max}+2)$-point Gauss quadrature with $I_{\rm max}$=10. This corresponds to taking six different orientation angles.[21] The contributions from each eigenbarrier are shown by the dashed lines in Fig. 8. The solid line is the sum of all the contributions, which is compared with the experimental data.[18] One can see that the calculation well reproduces the experimental data. Moreover, this analysis suggests that ^{154}Sm is a prolately deformed nucleus, since if it were an oblate nucleus, then lower potential barriers would have larger weights and $D_{\rm fus}$ would be larger for smaller E, in contradiction to the experimentally observed barrier distribution.[13]

The fusion barrier distribution has been extracted for many systems, see Ref. 13) and references therein. The extracted barrier distributions were shown to be sensitive to the effects of channel couplings and have provided a much clearer way of understanding their effects on the fusion process than the fusion excitation functions

themselves. These experimental data have thus enabled a detailed study of the effects of nuclear intrinsic excitations on fusion reactions and have generated renewed interest in heavy-ion subbarrier fusion reactions. An important point is that the nature of subbarrier fusion reactions as a tunneling process exponentially amplifies the effects of the details of the nuclear structure. The fusion barrier distribution makes these effects even more visible when it is plotted in a linear scale. The subbarrier fusion reactions thus offer a novel way of nuclear spectroscopy, which could be called tunneling-assisted nuclear spectroscopy. As an example, it was recently applied to elucidate the shape transition and shape coexistence of Ge isotopes.[91),92)] It is worthwhile to also mention that the method of the barrier distribution has been successfully applied to heavy-ion quasi-elastic scattering.[63),93)]

4.3. *Eigenchannel representation*

As we have discussed in the previous subsection, the barrier distribution representation, that is, the second derivative of $E\sigma_{\rm fus}$, has a clear physical meaning only if the excitation energy of the intrinsic motion is zero. The concept holds only approximately when the excitation energy is finite. Nonetheless, this analysis has been successfully applied to systems with relatively large excitation energies.[18),79),94)] For example, the second derivative of $E\sigma_{\rm fus}$ for the ^{16}O + ^{144}Sm fusion reaction has a clear double-peak structure (see the right panel of Fig. 8).[18),94)] The coupled-channels calculation also yields a similar double-peak structure of the fusion barrier distribution, and this structure has been interpreted in terms of the anharmonic octupole phonon excitations in ^{144}Sm,[72),73)] whose excitation energy is 1.8 MeV for the first 3^- state. Also the analysis of the fusion reaction between ^{58}Ni and ^{60}Ni, where the excitation energies of quadrupole phonon states are 1.45 and 1.33 MeV, respectively, shows that the barrier distribution representation depends strongly on the number of phonon states included in coupled-channels calculations.[79)] These analyses suggest that the representation of the fusion process in terms of the second derivative of $E\sigma_{\rm fus}$ is a powerful method to study the details of the effects of the nuclear structure, irrespective of the excitation energy of the intrinsic motion.

When the excitation energy of the intrinsic motion is finite, the barrier distribution can be still defined in terms of the eigenchannels. To illustrate this, first note that Eq. (3·15) can be expressed as

$$P(E) = (T^\dagger T)_{n_i n_i}, \tag{4·9}$$

using the completeness of the channels n (we have suppressed the index J). We then introduce the eigenfunctions of the Hermitian operator $T^\dagger T$ as

$$(T^\dagger T)|\phi_k\rangle = \gamma_k|\phi_k\rangle. \tag{4·10}$$

Using this basis, the penetrability is given by

$$P(E) = \sum_k |\langle\phi_k|n_i\rangle|^2 \cdot \gamma_k. \tag{4·11}$$

When the excitation energies ϵ_n are all zero, as we have discussed in §4.1, one can diagonalize the coupling matrix $V_{nn'}(r)$ with the basis set which is independent of

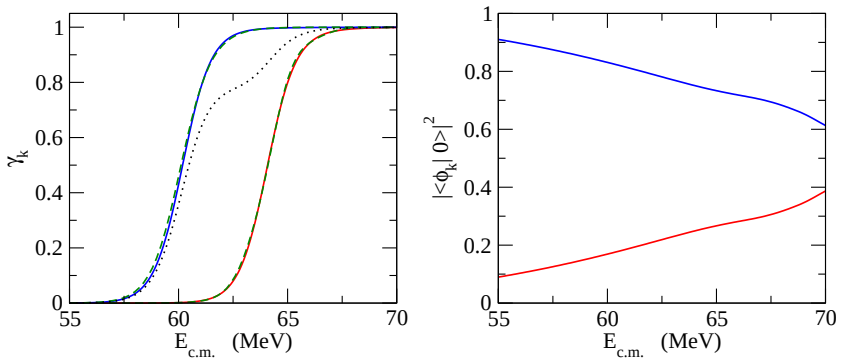

Fig. 9. (Left panel) s-wave penetrabilities for the ^{16}O+^{144}Sm reaction. The dotted line is obtained with the coupled-channels calculations with a single-octupole phonon excitation in ^{144}Sm at 1.81 MeV with $\beta_3 = 0.205$. The solid lines show the eigenvalues of the square of the transmission matrix, $T^\dagger T$, defined by Eq. (4·10). The dashed lines denote the penetrabilities of the eigenbarriers constructed by diagonalizing the coupling matrix at each r. (Right panel) Weight factors $|\langle\phi_k|n_i\rangle|^2$ defined in Eq. (4·11) as a function of energy.

the radial coordinate r. In this case, the matrix T is diagonal for this basis, and the weight factor $|\langle\phi_k|n_i\rangle|^2$ is independent of E. Equation (4·11) is a generalization of this scheme, which is also applicable when the excitation energies are nonzero.

Figure 9 shows the two eigenvalues γ_k and the corresponding weight factors $|\langle\phi_k|n_i\rangle|^2$ as a function of E for a single-phonon coupling calculation for the s-wave ^{16}O+^{144}Sm reaction. To this end, we have taken into account couplings to the single-octupole phonon state in ^{144}Sm at 1.81 MeV with the deformation parameter of β_3 = 0.205. The total probability $P(E)$, and the penetrability of the two eigenbarriers, obtained by diagonalizing the coupling matrix $V_{nn'}(r)$ at each r, are also shown in the left panel of the figure by the dotted and dashed lines, respectively. One can see that the two eigenvalues γ_k approximately correspond to the penetrability of the eigenbarriers, and thus the factors $|\langle\phi_k|n_i\rangle|^2$ can be interpreted as the weight factors for each eigenbarrier. This implies that the fusion cross sections are still given by Eq. (4·2) even when the excitation energy is finite, except that the eigenbarriers are now constructed by diagonalizing the coupling matrix at each r. The weight factors do not vary strongly as a function of energy, suggesting that the concept of the fusion barrier distribution is still a good approximation even when the excitation energy of the intrinsic motion is finite. We have already reached the same conclusion in Ref. 95) using a different method from the one in this subsection. In contrast to the method in Ref. 95), the method in this subsection is more general since the applicability is not restricted to a two-level problem.

4.4. *Adiabatic potential renormalization*

Given that the concept of the fusion barrier distribution still holds even with a finite excitation energy, it is interesting to investigate how the fusion barrier distribution evolves as the excitation energy is varied. To this end, we carry out coupled-channels calculations for the ^{16}O+^{144}Sm reaction by taking into account the single-octupole phonon excitation in ^{144}Sm. The solid line in Fig. 10(a) shows the fusion

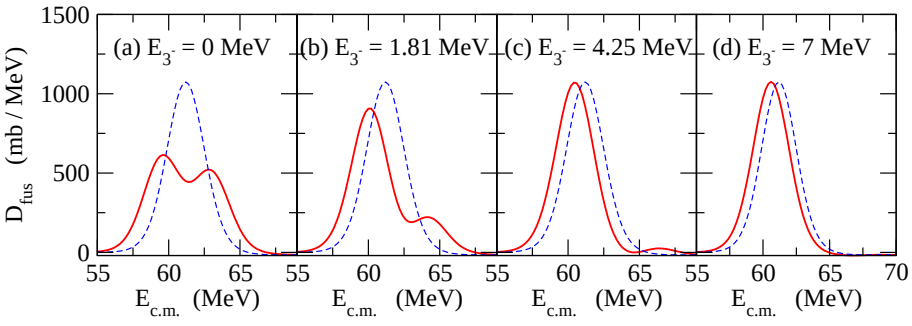

Fig. 10. Fusion barrier distribution $D_{\rm fus}$ for the ^{16}O+^{144}Sm reaction with several values of excitation energy, E_{3^-}, of the octupole vibration in ^{144}Sm. The solid lines are the results of the coupled-channels calculations, which take into account the single-octupole phonon excitation in ^{144}Sm, while the dashed lines are obtained without taking into account the channel coupling effect. The curvature $\hbar\Omega$ of the Coulomb barrier is 4.25 MeV in these calculations.

barrier distribution $D_{\rm fus}$ when the excitation energy of the octupole vibration, E_{3^-}, is set to zero. For comparison, the figure also shows the result of the no-coupling calculation by the dashed line. In this case, the original single barrier splits into two eigenbarriers with equal weight, one corresponds to the effective channel $|0^+\rangle + |3^-\rangle$ and the other corresponds to $|0^+\rangle - |3^-\rangle$. The fusion barrier distribution is slightly asymmetric since the barrier positions, R_b, are different between the two effective channels (see Eq. (4·7)).

Figure 10(b) corresponds to the physical case of $E_{3^-} = 1.81$ MeV. In this case, the barrier distribution still has a clear double-peak structure as in the experimental data,[18),94)] but the lower energy barrier acquires more weight and the barrier distribution is highly asymmetric. The effective channels are now $\alpha|0^+\rangle + \beta|3^-\rangle$ (the lower energy barrier) and $\beta|0^+\rangle - \alpha|3^-\rangle$ (the higher energy barrier) with $\alpha > \beta > 0$.

Figure 10(c) corresponds to the case where the excitation energy is set equal to the barrier curvature, $\hbar\Omega$, which is 4.25 MeV in the present calculations. In this case, the lower energy barrier has an appreciable weight although the weight factor for the higher energy barrier is not negligible. When the excitation energy is further increased, the weight for the lower energy barrier becomes close to unity, as is shown in Fig. 10(d), and the fusion cross sections are approximately given by

$$\sigma_{\rm fus}(E) = \sigma_{\rm fus}(E; V(r) + \lambda_0(r)), \tag{4·12}$$

where $V(r) + \lambda_0(r)$ is the lowest eigenbarrier (see Eq. (4·2)). Therefore, the main effect of the coupling to a state with a large excitation energy is to simply introduce an energy-independent shift of the potential, $V(r) \to V(r)+\lambda_0(r)$. This phenomenon is called the adiabatic potential renormalization.[96)–98)] Typical examples in nuclear fusion include the couplings to the octupole vibration in ^{16}O at 6.13 MeV[99)] and to giant resonances in general.

In Refs. 97) and 98), it has been argued on the basis of a path integral approach to multidimensional tunneling that the transition from sudden tunneling to adiabatic tunneling takes place at an excitation energy around the barrier curvature, $\hbar\Omega$. That is, if the excitation energy is much larger than the barrier curvature, the

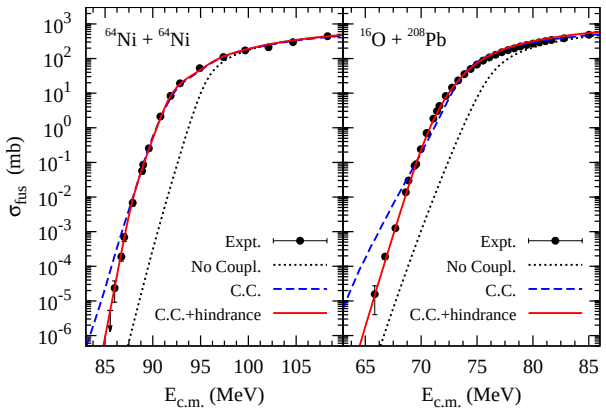

Fig. 11. Fusion cross sections for the ^{64}Ni+^{64}Ni and ^{16}O+^{208}Pb systems as a function of the incident energy. The experimental data are taken from Refs. 100) and 104). The dotted and dashed lines are the results of potential model and standard coupled-channels calculations, respectively. The solid lines denote the result when the hindrance of fusion cross sections at deep-subbarrier energies is described in the adiabatic model.[108)]

channel coupling effect can be well expressed in terms of the adiabatic barrier renormalization. The numerical calculations shown in Fig. 10 are consistent with this criterion.

§5. Fusion at deep-subbarrier energies and dissipative tunneling

Although the coupled-channels approach has been successful for heavy-ion reactions, many new challenges have been recognized in recent years. One of them is the surface diffuseness anomaly discussed in §2.1. Another challenge, which may also be related to the surface diffuseness anomaly,[46)] is the inhibition of fusion cross sections at deep subbarrier energies. This is a phenomenon found only recently, when fusion cross sections became measurable for several systems down to extremely low cross sections up to the level of a few nanobarn (nb).[100)–104)] These experimental data have shown that fusion cross sections systematically fall off much more steeply at deep-subbarrier energies with decreasing energy compared with the expected energy dependence of cross sections around the Coulomb barrier. That is, the experimental fusion cross sections appear to be hindered at deep-subbarrier energies compared with the standard coupled-channels calculations that reproduce the experimental data at subbarrier energies, although the fusion cross sections are still enhanced with respect to the prediction of a single-channel potential model.

Two different models have been proposed so far in order to account for the deep-subbarrier fusion hindrance. As the first model, assuming the frozen densities in the overlapping region (i.e., the sudden approximation), Misicu and Esbensen have introduced a repulsive core to an internucleus potential, which originates from the Pauli exclusion principle.[105)] See also Ref. 106) for a related publication. The resultant potential is much shallower than the standard potentials and hinders the

fusion probability for high partial waves. As the second model, on the other hand, Ichikawa et al. have proposed an adiabatic approach by assuming the formation of a neck between the colliding nuclei in the overlap region.[107),108)] In this model, the reaction is assumed to take place slowly so that the density distribution has enough time to adjust to the optimized distribution. In this adiabatic model, the hindrance of fusion cross sections origninates from the tunneling of a thick one-body potential due to the neck formation. This model has achieved comparably good reproduction of the experimental data to the sudden model, as is shown in Fig. 11.

The mechanism for the deep-subbarrier hindrance of fusion cross sections has not yet been fully understood, as the two different models, in which the origins of the deep-subbarrier hindrance are considerably different from each other, account for the experimental data equally well. However, there is a certain conclusion that can be reached by analyzing the threshold behavior in deep-subbarrier fusion,[100),101),109)–111)] independent of the fusion model.[110)] In Refs. 100), 101), and 109), the deep-subbarrier hindrance of fusion cross sections has been analyzed using the astrophysical S factor. It has been claimed that deep-subbarrier hindrance of fusion cross sections occurs at the energy at which the astrophysical S factor reaches its maximum. The authors of Refs. 100), 101), and 109) even parameterized the threshold energy as a function of the charge and mass numbers of the projectile and target nuclei. The relationship between the threshold for deep-subbarrier hindrance of fusion cross sections and the maximum of the S factor is not clear physically, and thus it is not trivial how to justify the identification of the threshold energy with the maximum of the astrophysical S factor. Nevertheless, it has turned out that the threshold energy thus obtained closely follows the values of phenomenological internucleus potentials at the touching configuration.[110)] This strongly indicates that the dynamics that takes place after the colliding nuclei touch each other somehow makes the astrophysical S factor decrease as the incident energy decreases, leading to the fusion hindrance phenomenon. Note that the fusion potential is almost the same between the sudden model and the adiabatic model before the touching (see Fig. 1 in Ref. 110)).

One important aspect of fusion reactions at deep-subbarrier energies is that the inner turning point of the potential may be located far inside the touching point of the colliding nuclei (see Fig. 1). After the two nuclei touch each other, many noncollective excitations of the unified one-body system are activated. As is well known from the Caldeira-Leggett model, couplings to these excitations lead to energy dissipation, which inhibits the tunneling probability.[10)] The energy dissipation may also occur before the touching as a consequence of particle transfer processes to highly excited states in the target nucleus.[112)] The phenomenon of deep-subbarrier fusion hindrance may therefore be a realization of dissipative quantum tunneling, which has been extensively studied in many fields of physics and chemistry. A characteristic feature in nuclear fusion, which is absent or may not be important in dissipative tunneling in other fields, is that the couplings to (internal) environmental degrees of freedom gradually occur [*)]. That is, before the touching, the fully

[*)] We thank M. Dasgupta and D.J. Hinde for discussions on this point.

quantum mechanical coupled-channels approach with couplings to a few collective states of separate nuclei is adequate, which however gradually loses its validity after the touching point owing to the dissipative couplings.[104] This is the region that the conventional coupled-channels approach does not treat explicitly by introducing an absorbing potential or by imposing the IWBC. Although it is highly important to construct a model for nuclear fusion by taking into account the dissipative couplings[108),113),114] in order to clarify the deep-subbarrier fusion hindrance, it is still a challenging open problem to do so. To this end, the transition from the excitations of two separate nuclei in the entrance channel, which are included in the conventional coupled-channels calculations, to *molecular* excitations (i.e., the excitations of the combined mono-nuclear system) has to be described in a consistent and smooth manner.[108),115)–117] The development of quantum mechanical versions of phenomenological classical models for deep inelastic collisions (DICs), such as the wall and window formulas for nuclear friction,[118)–120] will also be important in this respect.

§6. Application of barrier distribution method to surface physics

The barrier distribution method discussed in §4 is applicable not only to heavy-ion subbarrier fusion reactions but also to any multichannel tunneling problem. In general, the barrier distribution is defined as the first derivative of penetrability with respect to energy, dP/dE (see Eq. (4·7)).

As an application of the barrier distribution method developed in nuclear physics to other fields, let us discuss the dissociative adsorption process of diatomic molecules on a metal surface. When molecular beams are injected on a certain metal, such as Cu or Pd, diatomic molecules are broken up in the vicinity of the metal surface to form two atoms owing to the molecule-metal interactions before they adhere to the metal. This process is referred to as dissociative adsorption, and has been extensively studied in surface science together with the inverse process, that is, associative desorption.[121] The adsorption process takes place by quantum tunneling at low incident energies, as there is a potential barrier between the two phases of the molecules, i.e., the molecular phase and the breakup phase with two separate atoms.[121),122] The vibrational and rotational excitations of diatomic molecules play an important role in dissociative adsorption,[123)–125] as in heavy-ion subbarrier fusion reactions. The coupled-channels method has been utilized to discuss the effects of the internal excitations of molecules on dissociative adsorption.[126)–133]

In this section, we discuss only the simplest case, that is, the effect of the rotational excitation on dissociative adsorption, while the vibrational degrees of freedom are assumed to be frozen in the ground state. In contrast to heavy-ion fusion reactions, the initial rotational state in the problem of dissociative adsorption is not necessarily the ground state. The initial rotational state of diatomic molecules in molecular beams can in fact be selected, and the experimental data of Michelsen et al.[124),125] have indicated that the adsorption probability of D_2 molecules on a Cu surface shows nonmonotonic behavior as a function of the initial rotational state. That is, at a given incident energy, starting from the initial rotational state $L_i = 0$,

the adsorption probability first decreases for $L_i = 5$ and then increases for $L_i = 10$ and $L_i = 14$ (see Fig. 9 in Ref. 125)).

In order to explain this behavior, Diño et al. have considered a simple Hamiltonian for H_2 and D_2 molecules given by[129),131)]

$$H(s,\theta) = -\frac{\hbar^2}{2M}\frac{\partial^2}{\partial s^2} + \frac{\hbar^2}{2I(s)}\hat{\boldsymbol{L}}^2 + V(s,\theta), \tag{6·1}$$

where s is the one-dimensional reaction path in the two-dimensional potential energy surface spanned by the molecule-surface distance, Z, and the interatomic distance, r. The reaction takes place from $s = -\infty$, which corresponds to the approaching phase of molecules, to $s = +\infty$, where the incident molecule has broken up to form two atoms. The sticking probability to the metal surface is identified as the penetrability of the potential barrier, V. M in Eq. (6·1) is the mass for the translational motion of the diatomic molecule given by $M = 2m$, where m is the mass of the atom (i.e., $m = m_H$ for a H_2 molecule and $m = m_D$ for a D_2 molecule). θ is the molecular orientation angle, where θ=0 corresponds to the configuration of the molecule perpendicular to the surface while $\theta = \pi/2$ corresponds to the configuration parallel to the surface. $\hat{\boldsymbol{L}}$ is the associated angular momentum operator. $I(s)$ is the momentum inertia for the rotational motion given by

$$I(s) = \mu r_0^2(1 + fe^{\alpha s}), \tag{6·2}$$

where $\mu = m/2$ and f is a parameter characterizing the s dependence of the interatomic distance r, r_0 being the interatomic distance for an isolated molecule. The same parameter α as that in Eq. (6·2) also appears in the potential energy, $V(s,\theta)$, which is parameterized as

$$V(s,\theta) = \frac{E_a}{\cosh^2(\alpha s)}(1 - \beta\cos\theta^2) + V_1\cos^2\theta\cdot\frac{1}{2}(1 + \tanh(\alpha s)), \tag{6·3}$$

$$\equiv V_0(s) + V_2(s)Y_{20}(\theta), \tag{6·4}$$

with

$$V_0(s) = \frac{E_a}{\cosh^2(\alpha s)}\left(1 - \frac{\beta}{3}\right) + \frac{V_1}{6}(1 + \tanh(\alpha s)), \tag{6·5}$$

$$V_2(s) = -\frac{E_a}{\cosh^2(\alpha s)}\cdot\frac{2\beta}{3}\sqrt{\frac{4\pi}{5}} + \frac{1}{3}\sqrt{\frac{4\pi}{5}}V_1(1 + \tanh(\alpha s)). \tag{6·6}$$

The coupled-channels equations for the Hamiltonian (6·1) can be derived in the same manner as in §3. For scattering with the initial rotational angular momentum of molecules of L_i and its z-component M_i, we expand the total wave function as

$$\Psi_{L_iM_i}(s,\theta) = \sum_L \phi_{LL_i}(s)Y_{LM_i}(\theta). \tag{6·7}$$

Note that the Hamiltonian (6·1) conserves the value of M_i, as the coupling potential

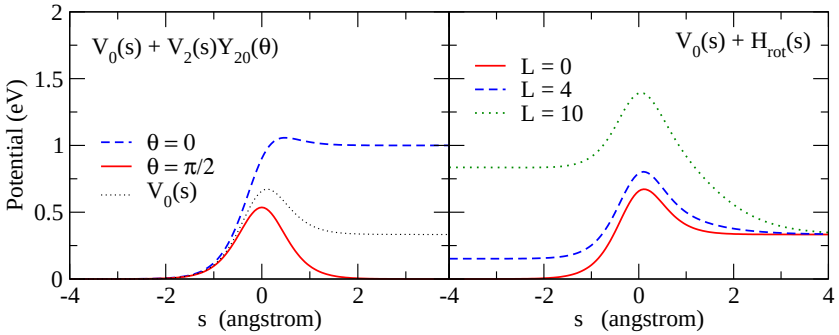

Fig. 12. Potential energy for dissociative adsorption process of H_2 molecule on metal surface given by Eq. (6·4). The parameters are E_a=0.536 eV, V_1=1.0 eV, α=1.5 Å^{-1}, $\beta = 0.25$, r_0=0.739 Å, and $f = 0.14$. The left panel shows the potential for $L = 0$ as a function of the reaction path coordinate s for $\theta = 0$ (dashed line) and $\theta = \pi/2$ (solid line), where θ is the molecular orientation angle (θ=0 and $\theta = \pi/2$ correspond to the configurations with the molecule perpendicular and parallel to the metal surface, respectively) and $\hat{\boldsymbol{L}}$ is the associated angular momentum operator. The spherical part of the potential, $V_0(s)$, is also shown by the dotted line. The right panel shows the sum of the spherical part of the potential, $V_0(s)$, and the rotational energy, $H_{\rm rot}(s) = L(L+1)\hbar^2/2I(s)$, for three different values of L.

is proportional to $Y_{20}(\theta)$. The coupled-channels equations then become

$$\left[-\frac{\hbar^2}{2M}\frac{d^2}{ds^2} + \frac{L(L+1)\hbar^2}{2I(s)} + V_0(s) - E\right]\phi_{LL_i}(s) + V_2(s)\sum_{L'}\langle Y_{LM_i}|Y_{20}|Y_{L'M_i}\rangle\phi_{L'L_i}(s), \tag{6·8}$$

where the matrix element $\langle Y_{LM_i}|Y_{20}|Y_{L'M_i}\rangle$ is given by

$$\langle Y_{LM_i}|Y_{20}|Y_{L'M_i}\rangle = (-)^{M_i}\sqrt{\frac{5}{4\pi}}\sqrt{(2L+1)(2L'+1)}\begin{pmatrix} L & 2 & L' \\ 0 & 0 & 0 \end{pmatrix}\begin{pmatrix} L & 2 & L' \\ -M_i & 0 & M_i \end{pmatrix}. \tag{6·9}$$

Noting that $I(s) \to \mu r_0^2$ for $s \to -\infty$ and $I(s) \to 0$ for $s \to \infty$, these coupled-channels equations are solved by imposing the boundary conditions of

$$\phi_{LL_i}(s) = e^{ik_L s}\delta_{L,L_i} - \sqrt{\frac{k_{L_i}}{k_L}}\,R_{LL_i}e^{-ik_L s}, \qquad (s \to -\infty) \tag{6·10}$$

$$= \sqrt{\frac{k_{L_i}}{k}}\,T_{LL_i}e^{iks}, \qquad (s \to \infty) \tag{6·11}$$

where $k_L = \sqrt{2M(E-\epsilon_L)/\hbar^2}$ with $\epsilon_L = L(L+1)\hbar^2/2\mu r_0^2$ and $k = \sqrt{2ME/\hbar^2}$. The adsorption probability for given values of L_i and M_i is then obtained as

$$P_{L_iM_i} = \sum_L |T_{LL_i}|^2. \tag{6·12}$$

By averaging over all possible M_i, the total adsorption probability for L_i is given by

$$P_{L_i} = \frac{1}{2L_i+1}\sum_{M_i} P_{L_iM_i}. \tag{6·13}$$

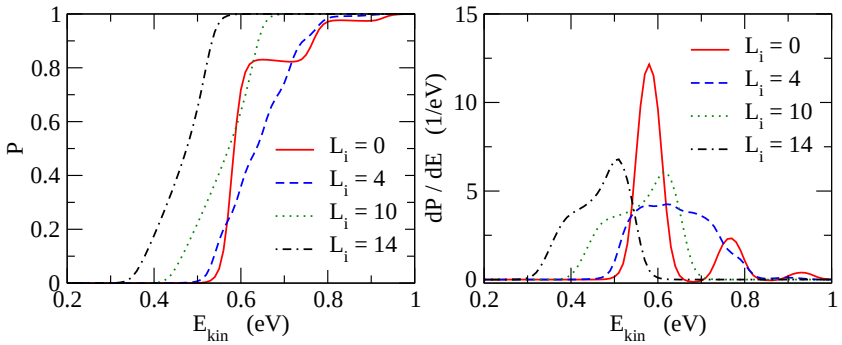

Fig. 13. Results of the coupled-channels calculation for the dissociative adsorption process of H_2 molecules. The left panel shows the adsorption probability, P, while the right panel shows the barrier distribution, defined as dP/dE, for several values of the initial angular momenta L_i for the rotational state of the molecule as a function of the initial kinetic energy $E_{\rm kin}$.

Let us now solve the coupled-channels equations for H_2 molecules. The results are qualitatively the same for D_2 molecules. Following Ref. 129), we take E_a=0.536 eV, V_1=1.0 eV, α=1.5 Å^{-1}, $\beta = 0.25$, and r_0=0.739 Å. For the factor f in Eq. (6·2), we take $f = 0.14$.[134] The potential with these parameters is shown in Fig. 12. The left panel shows the potential energy $V(s,\theta)$ given by Eq. (6·4) for two different values of θ. For comparison, the figure also shows the spherical part of the potential, $V_0(s)$. One can see that the barrier is lower for the configuration parallel to the metal surface (that is, $\theta = \pi/2$) than for the configuration perpendicular to the surface, $\theta = 0$. The right panel, on the other hand, shows the sum of the spherical part of the potential, $V_0(s)$, and the rotational energy, $H_{\rm rot}(s) = L(L+1)\hbar^2/2I(s)$, for three different values of L. Because of the s dependence of the rotational moment of inertia, $I(s)$, the barrier height for the molecules incident from $s = -\infty$, that is, the difference between the energy at $s = 0$ and that at $s = -\infty$, decreases as a function of L.

The results of the coupled-channels calculations are shown in Fig. 13 for several values of the initial rotational state, L_i, in which the adsorption probability is plotted as a function of the incident kinetic energy of the molecule, defined as $E = E_{\rm kin} + L_i(L_i+1)\hbar^2/2r_0^2$. As has been noted in Refs. 129) and 131), these calculations well account for the nonmonotonic behavior of the adsorption probability as a function of L_i. The right panel shows the corresponding barrier distribution, dP/dE, obtained with the point difference formula with an energy step of 0.03 eV. One can clearly see different structures for each L_i. For $L_i = 0$, the barrier distribution has three prominent peaks. These peaks are smeared for $L_i = 4$, and at the same time, the center of mass of the distribution is shifted towards a higher energy, leading to the decrease in adsorption probability. This is due to the fact that the result for $L_i = 4$ is actually given by the average over contributions from nine different M_i values. In order to demonstrate this effect, Fig. 14 shows the results of the single-channel calculations for $L_i = 2$ with three different values of M_i and their average. For comparison, the figure also shows the single-channel calculation for $L_i = 0$ (dotted line). We define the single-channel calculation as that which neglects

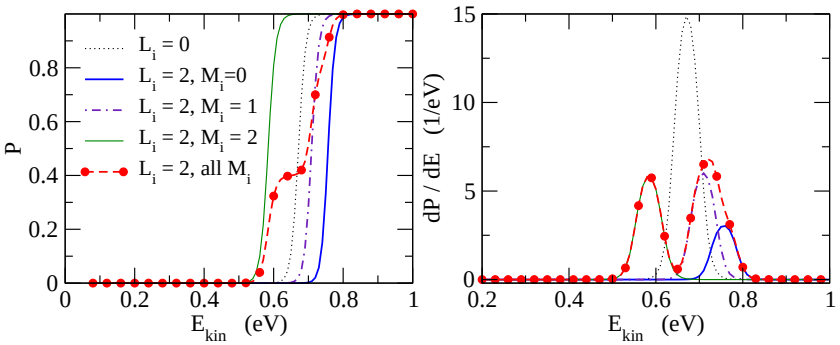

Fig. 14. Results of the single-channel calculation obtained by neglecting all the coupling matrix elements in the coupled-channels equations except for the diagonal component. The left and right panels show the adsorption probability, P, and the barrier distribution, dP/dE, respectively. The dotted lines denote the results when the initial rotational state is at $L_i = 0$. The thin solid, dot-dashed, and thick solid lines are the results of $(L_i, M_i) = (2,0), (2,1)$, and (2,2), respectively. The dashed lines with the solid circles show the results for $L_i = 2$ obtained by averaging all the M_i components. The barrier distributions shown in the right panel are multiplied by the weight factors of 1/5 (for $M_i = 0$) and 2/5 (for $M_i = 1$ and 2).

all the coupling terms in the coupled-channels equations (6·8) except for the diagonal term, $L = L'$. Because of the properties of the spherical harmonics, the diagonal term of the coupling potential is attractive for $M_i = 2$, while it is repulsive for $M_i = 0$ and 1 (see Eq. (6·9)). The single peak in the barrier distribution for $L_i = 0$ is then becomes three peaks in the case of $L_i = 4$, shifting the center of mass of the distribution towards a slightly higher energy (note that $-M_i$ gives the same contribution as M_i). With the off-diagonal components of the coupling potential, the distribution will be further smeared, as in the distribution for $L_i = 4$ shown in Fig. 13. When the initial angular momentum is further increased, the barrier distribution starts moving towards lower energies, as seen in the figure for $L_i = 10$ and 14, which enhances the adsorption probability as a consequence. This is mainly due to the fact that the barrier is lowered for a large value of the rotational state, L_i, as has been shown in Fig. 12.

The barrier distribution representation of the tunneling probability provides a useful means to understand the underlying dynamics of the dissociative adsorption process as the shape of the distribution strongly reflects the intrinsic molecular motions. This is particularly the case when the rotational and vibrational degrees are taken into account simultaneously.[130),132)] It will be an interesting future study to investigate how the barrier distribution behaves in the presence of rotational excitation together with vibrational excitation.

§7. Summary and outlook

Recent developments in experimental techniques have enabled high-precision measurements of heavy-ion fusion cross sections. Such high-precision experimental data have elucidated the mechanism of subbarrier fusion reactions in terms of the

quantum tunneling of systems with many degrees of freedom. In particular, the effects of the coupling of the relative motion between the target and projectile nuclei to their intrinsic excitations have been transparently clarified through the barrier distribution representation of fusion cross sections.

The effects of channel coupling can be taken into account most naturally with the coupled-channels method. When the excitation energy of an intrinsic motion coupled to the relative motion is zero, the concept of the barrier distribution holds exactly. In this case, quantum tunneling takes place much faster than the intrinsic motion. The effects of the couplings can then be expressed in terms of the distribution of potential barriers, and the fusion cross sections are given as a weighted sum of the fusion cross sections for the distributed barriers. The underlying structure of the barrier distribution can be most clearly investigated when the first derivative of barrier penetrability, dP/dE, is plotted as a function of energy. In heavy-ion fusion reactions, this quantity corresponds to the second derivative of $E\sigma_{\rm fus}$, which is referred to as the fusion barrier distribution, $D_{\rm fus}$. The fusion barrier distribution has been extracted for many systems through the high-precision experimental data of fusion cross sections, $\sigma_{\rm fus}$.

Even when the excitation energy of the intrinsic motion is not zero, the concept of the fusion barrier distribution can be approximately generalized using the eigenchannel representation of the nuclear S-matrix, defined as the eigenstates of $S^\dagger S$. We have demonstrated that the barrier distribution shows a transition from the sudden tunneling limit to the adiabatic tunneling limit in a natural way as the excitation energy increases, where the potential is simply renormalized in the latter limit without affecting the shape of the barrier distribution (i.e., adiabatic barrier renormalization).

The barrier distribution representation is also applicable to other multichannel quantum tunneling problems. A good example is the dissociative adsorption phenomenon in surface science. The rotational and vibrational excitations of diatomic molecules play an important role in the adsorption process. These effects can be described by the coupled-channels approach, and the barrier distribution can be defined as in heavy-ion subbarrier fusion reactions. The results of coupled-channels calculations have indicated that the barrier distribution representation provides a useful means of clarifying the underlying mechanism in the dynamics of the surface interaction of molecules.

Although our understanding of subbarrier fusion reactions has considerably increased in the past decades, there are still many open problems in heavy-ion subbarrier fusion reactions. For example, it has not yet been understood completely how the hindrance of fusion cross sections with respect to the standard coupled-channels calculation takes place at deep-subbarrier energies. A likely mechanism of the hindrance is that many noncollective channels are activated after the target and projectile nuclei overlap with each other, and the relative energy is irreversibly dissipated to the intrinsic motions. This would occur only at deep-subbarrier energies, in which the inner turning point of the potential barrier is located inside the touching radius of the two nuclei. This phenomenon may thus be a good example of dissipative quantum tunneling, which has been extensively discussed in many fields

of physics and chemistry. A unique feature in nuclear physics is that the dissipative nature of the couplings gradually appears, in a sense that the coupling is reversible before the touching and it gradually reveals the irreversible character as the overlap of the colliding nuclei increases. In order to gain a deep insight into this problem, it might be helpful to revisit heavy-ion DICs from a more quantum mechanical point of view. This is also important in connection with the synthesis of superheavy elements by heavy-ion collisions with large mass numbers, for which the fusion cross section is strongly hindered at energies near the bare Coulomb barrier.

Other important issues not covered in this paper include the fusion of halo nuclei and the role of multinucleon transfer. For the former, there has been considerable debate concerning how the breakup process affects subbarrier fusion.[135)–141)] However, the interplay between fusion and breakup involves many complex processes[24)] and the role of breakup in fusion has not yet been understood completely. Moreover, particle transfer processes also affect both fusion and breakup in a nontrivial way, as has been found recently in ^{6,7}Li + ^{208}Pb reactions[142)] (see Ref. 143) for a review on subbarrier fusion of the weakly bound stable nuclei ^{6,7}Li and ^{9}Be). A theoretical calculation has to take into account the fusion, transfer, and breakup processes simultaneously in a consistent manner. It remains a challenging problem to carry out such calculations, although the time-dependent wave packet approach[140)] has been performed with a limited partition for the transfer channels. From the experimental side, fusion cross sections for many neutron-rich nuclei do not appear to show any particular enhancement or hindrance,[144)–147)] but recent experimental data for ^{12,13,14,15}C+^{232}Th reactions have shown that the fusion cross sections are enhanced for the ^{15}C projectile as compared with those for the other C isotopes.[148)] Again, several types of transfer channels would have to be considered to understand the differences in the behavior of fusion cross sections.[142),149)–151)] In particular, the multi-nucleon transfer process may play an important role in the fusion of neutron-rich nuclei. Although there have been a few attempts to treat the multineutron transfer process in subbarrier fusion reactions,[152)–157)] it is still a challenging problem to include the multinucleon transfer processes in a full quantum mechanical manner consistently with inelastic channels while also taking into account the final Q-value distribution of the transfer.

A much more challenging problem is to describe heavy-ion fusion reactions, and thus many-particle tunneling,[158)] from fully quantum many-body perspectives, starting from nucleon degrees of freedom. The time-dependent Hartree-Fock (TDHF) theory has been widely employed to microscopically describe nuclear dynamics.[159),160)] It is well known, however, that the TDHF method has a serious drawback in that it cannot describe a many-particle tunneling phenomenon. In order to solve this problem, Bonasera and Kondratyev have introduced imaginary time propagation.[161),162)] In relation to this, we wish to mention that an alternative imaginary time approach, called the mean field tunneling theory, for the quantum tunneling of systems with many degrees of freedom has been developed in Ref. 163). The mean field tunneling theory is a reformulation of the dynamical norm method for quantum tunneling,[86),164)] which evaluates the nonadiabatic effect on the tunneling rate through the change in the norm of the wave function for the intrinsic space during the evolution

along the imaginary time axis. The mean field tunneling theory has been applied to quantum mechanically discuss the effects of electron screening in low-energy nuclear reactions,[163] while the dynamical norm method has been used to discuss the effects of nuclear oscillation on fission.[164] It would be an interesting challenge to develop a fully microscopic version of these methods and apply them to heavy-ion fusion reactions. More recently, Umar et al. have used the density-constrained TDHF (DC-TDHF) method to analyze heavy-ion fusion reactions.[165–167] Even though these microscopic approaches seem promising, they are based on certain assumptions, such as a local collective potential with a single channel. It is thus not yet clear whether they are applicable to many-particle tunneling problems in general, such as two-proton radioactivity[168–173] and alpha decays.[174–178] An ultimate goal would be to develop a general microscopic theory that can describe several tunneling phenomena simultaneously, not only in nuclear physics but also in other fields of physics and chemistry. Such a theory would naturally provide a way to describe the role of irreversibility (that is, the energy and angular momentum dissipations) as well as the evolution of density after the touching in subbarrier fusion reactions without any assumption of the adiabaticity of the fusion process.

Acknowledgements

We thank D. M. Brink, A. B. Balantekin, N. Rowley, A. Vitturi, M. Dasgupta, D. J. Hinde, T. Ichikawa, M. S. Hussein, L. F. Canto, C. Beck, L. Corradi, A. Diaz-Torres, P. R. S. Gomes, S. Kuyucak, J. F. Liang, C. J. Lin, G. Montagnoli, A. Navin, G. Pollarolo, F. Scarlassara, A. M. Stefanini, and H. Q. Zhang for collaborations and many useful discussions. K.H. also thanks Y. Miura, T. Ichikawa, W. A. Diño, and S. Suto for useful discussions on dissociative adsorption in surface physics. This work was supported by the Japanese Ministry of Education, Culture, Sports, Science and Technology by a Grant-in-Aid for Scientific Research under program no. (C) 22540262.

Appendix A

—— Relationship between Surface Diffuseness and Barrier Parameters ——

In this appendix, we discuss the relationship between the surface diffuseness parameter a in a nuclear potential and the parameters that characterize the Coulomb barrer, that is, the curvature, the barrier height, and the barrier position. With such a relationship, one can estimate the value of a from empirical barrier parameters.

For a given nuclear potential $V_N(r)$, the barrier position R_b is obtained from the condition that the first derivative of the total potential is zero at $r = R_b$,

$$\frac{d}{dr}V(r)\bigg|_{r=R_b} = \left[\frac{dV_N(r)}{dr} - \frac{Z_P Z_T e^2}{r^2}\right]_{r=R_b} = 0. \tag{A·1}$$

The barrier height V_b and the curvature Ω are then evaluated as

$$V_b = V_N(R_b) + \frac{Z_P Z_T e^2}{R_b}, \tag{A·2}$$

$$\Omega = \sqrt{-\frac{V_N''(R_b) + 2Z_P Z_T e^2/R_b^3}{\mu}}, \tag{A·3}$$

where $V_N''(r)$ is the second derivative of the nuclear potential with respect to r.

A.1. *Exponential potential*

We first consider the exponential potential given by

$$V_N(r) = V_0 e^{-r/a}. \tag{A·4}$$

From Eq. (A·1), the depth of the nuclear potential V_0 is related to the charge product $Z_P Z_T$ as

$$-\frac{V_0}{a} e^{-R_b/a} - \frac{Z_P Z_T e^2}{R_b^2} = 0. \tag{A·5}$$

From this equation, the barrier height and the curvature are

$$V_b = \frac{Z_P Z_T e^2}{R_b}\left(1 - \frac{a}{R_b}\right), \tag{A·6}$$

$$\Omega^2 = \frac{Z_P Z_T e^2}{\mu R_b^2}\left(\frac{1}{a} - \frac{2}{R_b}\right), \tag{A·7}$$

respectively.

A.2. *Woods-Saxon potential*

We next consider the Woods-Saxon potential given by

$$V_N(r) = -\frac{V_0}{1 + e^{(r-R_0)/a}}. \tag{A·8}$$

Combining Eqs. (A·1), (A·2), and (A·3), one finds that the surface diffuseness parameter a is expressed in terms of R_b, V_b, and Ω as

$$a = \frac{R_b}{-\frac{\mu\Omega^2 R_b^3}{Z_P Z_T e^2} - 2 + \frac{2Z_P Z_T e^2}{Z_P Z_T e^2 - R_b V_b}}. \tag{A·9}$$

Once the surface diffuseness parameter is thus evaluated, the other two parameters in the nuclear potential can be obtained as

$$1 + e^{-x} = \frac{1}{a}\frac{R_b^2}{Z_P Z_T e^2}\left(\frac{Z_P Z_T e^2}{R_b} - V_b\right), \tag{A·10}$$

$$V_0 = a e^{-x}(1 + e^x)^2 \frac{Z_P Z_T e^2}{R_b^2}, \tag{A·11}$$

where x is defined as $(R_b - R_0)/a$.

Appendix B
—— Parabolic Approximation and the Wong Formula ——

If the Coulomb barrier is approximated by the parabola,

$$V(r) \sim V_b - \frac{1}{2}\mu\Omega^2(r-R_b)^2, \tag{B·1}$$

the corresponding penetrability can be evaluated analytically as

$$P(E) = \frac{1}{1+\exp\left[\frac{2\pi}{\hbar\Omega}(V_b-E)\right]}. \tag{B·2}$$

Using the parabolic approximation, Wong has derived an analytic expression for fusion cross sections.[49] He assumed that (i) the curvature of the Coulomb barrier, $\hbar\Omega$, is independent of the angular momentum l, and (ii) the position of the Coulomb barrier, R_b, is also independent of l, and the dependence of the penetrability on the angular momentum can be well approximated by shifting the incident energy as

$$P_l(E) = P_{l=0}\left(E - \frac{l(l+1)\hbar^2}{2\mu R_b^2}\right). \tag{B·3}$$

If many partial waves contribute to the fusion cross section, the sum in Eq. (2·17) may be replaced by the integral,

$$\sigma_{\rm fus}(E) = \frac{\pi}{k^2}\int_0^\infty dl\ (2l+1)P_l(E). \tag{B·4}$$

Changing the variable from l to $l(l+1)$, the integral can be explicitly evaluated, leading to the Wong formula[49]

$$\sigma_{\rm fus}(E) = \frac{\hbar\Omega}{2E}R_b^2 \ln\left[1+\exp\left(\frac{2\pi}{\hbar\Omega}(E-V_b)\right)\right]. \tag{B·5}$$

At energies well above the Coulomb barrier, this formula reduces to the classical expression of the fusion cross section given by Eq. (4·3).

The left panel of Fig. 15 shows the parabolic approximation to the Coulomb barrier for the ^{16}O + ^{144}Sm system shown in Fig. 1. Because of the long-range Coulomb interaction, the Coulomb barrier is asymmetric and the parabolic potential has a smaller width than the realistic potential. Nevertheless, the Wong formula for fusion cross sections, Eq. (B·5), works well except at energies well below the barrier, where the parabolic approximation breaks down (see the right panel of Fig. 15).

Even though the Wong formula appears to work well for the single-channel potential model, one can still discuss the corrections to it. The first correction is with respect to the integral in Eq. (B·4). To discuss the correction, we first note that replacing the sum in Eq. (2·17) with the integral in Eq. (B·4) is equivalent to taking only the leading term ($m=0$) of the exact Poisson sum formula,

$$\sigma_{\rm fus}(E) = \frac{\pi}{k^2}\sum_l (2l+1)P_l(E) = \frac{2\pi}{k^2}\sum_{m=-\infty}^{\infty}\int_0^\infty \lambda P(E;\lambda)e^{2\pi m i\lambda}d\lambda, \tag{B·6}$$

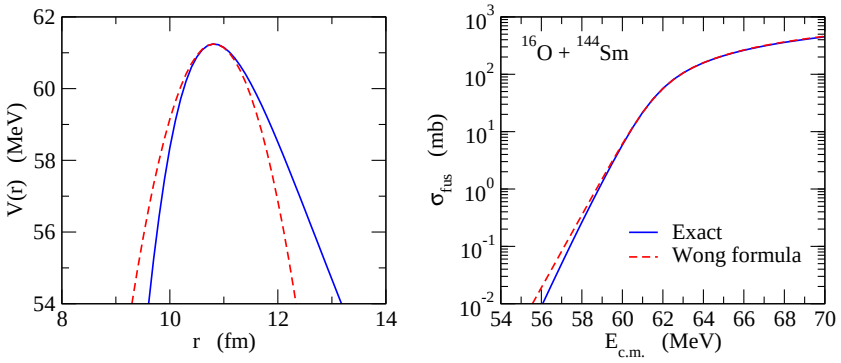

Fig. 15. (Left panel) Coulomb barrier for the ^{16}O+^{144}Sm system shown in Fig. 1 (solid line) and its parabolic approximation (dashed line). (Right panel) Comparison of the corresponding fusion cross sections obtained by numerically solving the Schrödinger equation without resorting to the parabolic approximation (solid line) and those obtained with the Wong formula, Eq. (B·5).

where $P(E;\lambda)$ is any smooth function of λ satisfying $P(E, l+1/2) = P_l(E)$.[81] Poffe et al. have evaluated the contribution of the next most important terms, $m = \pm 1$.[179] These terms lead to an oscillatory contribution to the fusion cross sections,

$$\sigma_{\rm fus}(E) = \sigma_W(E) + \sigma_{\rm osc}(E), \tag{B·7}$$

where $\sigma_W(E)$ is given by Eq. (B·5), while the oscillatory part $\sigma_{\rm osc}(E)$ is given by

$$\sigma_{\rm osc}(E) = 4\pi\mu R_b^2 \frac{\hbar\Omega}{k^2\hbar^2} \exp\left(-\frac{\pi\mu R_b^2\hbar\Omega}{l_g+\frac{1}{2}}\cdot\frac{1}{\hbar^2}\right)\sin(2\pi l_g). \tag{B·8}$$

Here, l_g is the grazing angular momentum satisfying

$$E = V(r) + \frac{l_g(l_g+1)\hbar^2}{2\mu R_b^2}. \tag{B·9}$$

For heavy systems, the oscillatory part of fusion cross sections, $\sigma_{\rm osc}$, is usually much smaller than the leading term, σ_W. However, for light symmetric systems such as ^{12}C+^{12}C, the oscillatory part becomes significant.[179)–183)] For a system of identical spin-zero bosons, the factor $(1+(-1)^l)$ has to be included in the sum in Eq. (2·17) owing to the symmetrization effect, making the contributions of all the odd partial waves vanish. In this case, the leading term of the fusion cross section is still given by the Wong formula, Eq. (B·5), while the oscillatory part becomes[179]

$$\sigma_{\rm osc}(E) = 4\pi\mu R_b^2 \frac{\hbar\Omega}{k^2\hbar^2} \exp\left(-\frac{\pi\mu R_b^2\hbar\Omega}{2l_g+1}\cdot\frac{1}{\hbar^2}\right)\sin(\pi l_g). \tag{B·10}$$

Figure 16 shows the fusion cross sections for the ^{12}C+^{12}C reaction obtained with a parabolic potential with $V_b = 5.6$ MeV, R_b=6.3 fm, and $\hbar\Omega = 3$ MeV. The solid line shows the result of the exact summation of partial wave contributions with Eq. (B·3), while the dashed line shows the sum of Eqs. (B·5) and (B·10). The separate

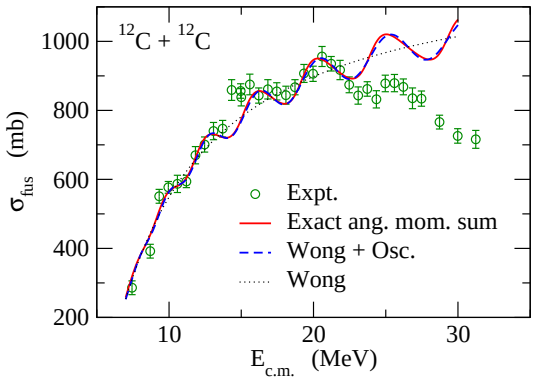

Fig. 16. Fusion excitation function for the ^{12}C+^{12}C system. The solid line is obtained by carrying out the exact angular momentum summation (with the symmetrization factor) in Eq. (2·17) with a parabolic potential with V_b = 5.6 MeV, R_b=6.3 fm, and $\hbar\Omega$ = 3 MeV. The barrier position and the curvature are assumed to be independent of the angular momentum l. The dotted line is obtained with the Wong formula, Eq. (B·5), while the dashed line is obtained as the sum of the Wong formula and the oscillatory cross sections given by Eq. (B·10). The experimental data are taken from Ref. 182).

contribution from the Wong formula, Eq. (B·5), is also shown by the dotted line. It can be seen that the oscillation of fusion cross sections can be well reproduced with the formula given by Eq. (B·10).

The second correction to the Wong formula is the angular momentum dependence of the barrier radius.[184] Up to the first order of $\hbar^2/\mu^2\Omega^2R_b^4$, Balantekin et al. have shown that the barrier radius for the lth partial wave R_{bl} is given by

$$R_{bl} = R_b - \frac{l(l+1)\hbar^2}{\mu^2\Omega^2R_b^3}. \tag{B·11}$$

This equation indicates that the barrier position decreases as the angular momentum l increases. At energies well above the barrier, the classical fusion cross sections are then modified to[184]

$$\sigma_{\rm fus}(E) = \pi R_b^2\left(1-\frac{V_b}{E}\right) - \frac{2\pi}{\mu\Omega^2E}(E-V_b)^2. \qquad (E \gg V_b) \tag{B·12}$$

Comparison between Eqs. (4·3) and (B·12) shows that the Wong formula slightly overestimates fusion cross sections at energies well above the Coulomb barrier.

Appendix C
—— *Multiphonon Coupling* ——

In this appendix, we show that the dimension of the coupled-channels equations can be reduced for vibrational couplings by introducing effective multiphonon channels. Suppose that we have two modes of vibrational excitations (e.g., quadrupole and octupole modes). We consider the excitation operator

$$\hat{O} = \beta_1(a_1^\dagger + a_1) + \beta_2(a_2^\dagger + a_2) \tag{C·1}$$

and the phonon Hamiltonian

$$H_0 = \hbar\omega_1 a_1^\dagger a_1 + \hbar\omega_2 a_2^\dagger a_2, \tag{C·2}$$

where $a_1^\dagger$ and $a_2^\dagger$ are the phonon creation operators for the first and second modes, respectively. β_i $(i = 1, 2)$ are the coupling constants, while $\hbar\omega_i$ $(i = 1, 2)$ are the phonon excitation energies for each mode. We have shifted the phonon energies so that the ground state is at zero energy.

If we truncate the phonon space up to the one-phonon states, we have three basis states, $|00\rangle, |10\rangle$, and $|01\rangle$, where the state $|n_1 n_2\rangle$ corresponds to the product state of the n_1 phonon state for the first mode and the n_2 phonon state for the second mode. Here, we have included the states with $n_1 + n_2 \leq 1$. The matrix elements of the operator $H_0 + \hat{O}$ with these basis states are,

$$H_0 + \hat{O} = \begin{pmatrix} 0 & \beta_1 & \beta_2 \\ \beta_1 & \hbar\omega_1 & 0 \\ \beta_2 & 0 & \hbar\omega_2 \end{pmatrix}. \tag{C·3}$$

It is easy to see that the ground state $|00\rangle$ couples only to a particular combination of $|10\rangle$ and $|01\rangle$,[69]

$$|\tilde{1}\rangle = \frac{1}{\sqrt{\beta_1^2 + \beta_2^2}} (\beta_1 |10\rangle + \beta_2 |01\rangle), \tag{C·4}$$

with

$$\hat{O}|00\rangle = \sqrt{\beta_1^2 + \beta_2^2}\, |\tilde{1}\rangle. \tag{C·5}$$

The other combination of $|10\rangle$ and $|01\rangle$, $\beta_2|10\rangle - \beta_1|01\rangle$, couples neither to $|00\rangle$ nor to $|\tilde{1}\rangle$, and this can be removed from the coupled-channels calculation if the excitation energies of the two modes are the same, $\hbar\omega_1 = \hbar\omega_2 \equiv \hbar\omega$. In this case, the dimension of the coupled-channels equations can be reduced to two with a modified strength as[69]

$$H_0 + \hat{O} = \begin{pmatrix} 0 & \bar{\beta} \\ \bar{\beta} & \hbar\omega \end{pmatrix}, \tag{C·6}$$

where $\bar{\beta}$ is defined by $\bar{\beta} = \sqrt{\beta_1^2 + \beta_2^2}$. One can easily generalize this scheme to higher members of phonon states. The resultant matrix is equivalent to that for a single-phonon mode with effective strength $\bar{\beta}$. For instance, when the phonon space is truncated at the two-phonon states, the coupling matrix is

$$H_0 + \hat{O} = \begin{pmatrix} 0 & \bar{\beta} & 0 \\ \bar{\beta} & \hbar\omega & \sqrt{2}\bar{\beta} \\ 0 & \sqrt{2}\bar{\beta} & 2\hbar\omega \end{pmatrix}, \tag{C·7}$$

where the effective two-phonon state is defined as

$$|\tilde{2}\rangle = \frac{1}{\beta_1^2 + \beta_2^2} \left(\beta_1^2 |20\rangle + \sqrt{2}\beta_1\beta_2 |11\rangle + \beta_2^2 |02\rangle \right). \tag{C·8}$$

References

1) G. Gamow, Z. Phys. **51** (1928), 204.
2) R. W. Gurney and E. U. Condon, Nature **122** (1928), 439; Phys. Rev. **33** (1929), 127.
3) P.L. Kapur and R. Peierls, Proc. Roy. Soc. London, Ser. A **163** (1937), 606.
4) T. Banks, C. M. Bender and T. T. Wu, Phys. Rev. D **8** (1973), 3346; Phys. Rev. D **8** (1973), 3366.
5) J. L. Gervais and B. Sakita, Phys. Rev. D **16** (1977), 3507.
6) D. M. Brink, M. C. Nemes and D. Vautherin, Ann. of Phys. **147** (1983), 171.
7) A. Schmid, Ann. of Phys. **170** (1986), 333.
8) S. Takada and H. Nakamura, J. Chem. Phys. **100** (1994), 98.
9) D. B. Schwartz, B. Sen, C. N. Archie, and J. E. Lukens, Phys. Rev. Lett. **55** (1985), 1547.
10) A. O. Caldeira and A. J. Leggett, Phys. Rev. Lett. **46** (1981), 211; Ann. of Phys. **149** (1983), 374.
11) *Proc. 4th Int. Symp. Foundations of Quantum Mechanics,* ed. M. Tsukada *et al.,* Japanese Journal of Applied Physics Series Vol. 9 (Publication Office of Japanese Journal of Applied Physics, Tokyo, 1993).
12) A. B. Balantekin and N. Takigawa, Rev. Mod. Phys. **70** (1998), 77.
13) M. Dasgupta, D. J. Hinde, N. Rowley and A. M. Stefanini, Annu. Rev. Nucl. Part. Sci. **48** (1998), 401.
14) M. Beckerman, Rep. Prog. Phys. **51** (1988), 1047; Phys. Rep. **129** (1985), 145.
15) S. G. Steadman and M. J. Rhoades-Brown, Annu. Rev. Nucl. Part. Sci. **36** (1986), 649.
16) W. Reisdorf, J. of Phys. G **20** (1994), 1297.
17) R. G. Stokstad, Y. Eisen, S. Kaplanis, D. Plete, U. Smilansky and I. Tserruya, Phys. Rev. Lett. **41** (1978), 465; Phys. Rev. C **21** (1980), 2427.
18) J. R. Leigh, M. Dasgupta, D. J. Hinde, J. C. Mein, C. R. Morton, R. C. Lemmon, J. P. Lestone, J. O. Newton, H. Timmers, J. X. Wei and N. Rowley, Phys. Rev. C **52** (1995), 3151.
19) C. H. Dasso, S. Landowne and A. Winther, Nucl. Phys. A **405** (1983), 381; Nucl. Phys. A **407** (1983), 221.
20) H. Esbensen, Nucl. Phys. A **352** (1981), 147.
21) M. A. Nagarajan, A. B. Balantekin and N. Takigawa, Phys. Rev. C **34** (1986), 894.
22) N. Rowley, G. R. Satchler and P. H. Stelson, Phys. Lett. B **254** (1991), 25.
23) J. X. Wei, J. R. Leigh, D. J. Hinde, J. O. Newton, R. C. Lemmon, S. Elfstrom, J. X. Chen and N. Rowley, Phys. Rev. Lett. **67** (1991), 3368.
24) L. F. Canto, P. R. S. Gomes, R. Donangelo and M.S. Hussein, Phys. Rep. **424** (2006), 1.
25) J. F. Liang and C. Signorini, Int. J. Mod. Phys. E **14** (2005), 1121.
26) P. Armbruster, Annu. Rev. Nucl. Part. Sci. **50** (2000), 411.
27) P. Armbruster and G. Münzenberg, Eur. Phys. J. H **37** (2012), 237.
28) G. R. Satchler and W. G. Love, Phys. Rep. **55** (1979), 183.
29) M. E. Brandan and G. R. Satchler, Phys. Rep. **285** (1997), 143.
30) D. T. Khoa and G. R. Satchler, Nucl. Phys. A **668** (2000), 3.
31) D. T. Khoa, G. R. Satchler and W. von Oertzen, Phys. Rev. C **56** (1997), 954.
32) D. T. Khoa, Phys. Rev. C **63** (2001), 034007.
33) B. Sinha, Phys. Rep. **20** (1975), 1.
34) B. Sinha and S. A. Moszkowski, Phys. Lett. B **81** (1979), 289.
35) R. A. Broglia and A. Winther, *Heavy-Ion Reactions* (Addison-Wesley, New York, 1991).
36) Ö. Akyüz and A. Winther, in *Nuclear Structure and Heavy-Ion Collisions,* Proc. Int. School of Physics "Enrico Fermi" Course LXXVII, Varenna, 1979, ed. R. A. Broglia et al. (North-Holland, Oxford, 1981).
37) K. Hagino, T. Takehi, A. B. Balantekin and N. Takigawa, Phys. Rev. C **71** (2005), 044612.
38) K. Washiyama, K. Hagino and M. Dasgupta, Phys. Rev. C **73** (2006), 034607.
39) L. R. Gasques et al., Phys. Rev. C **76** (2007), 024612.
40) M. Evers et al., Phys. Rev. C **78** (2008), 034614.
41) C. J. Lin et al., Phys. Rev. C **79** (2009), 064603.
42) J. O. Newton, C. R. Morton, M. Dasgupta, J. R. Leigh, J. C. Mein, D. J. Hinde, H. Timmers and K. Hagino, Phys. Rev. C **64** (2001), 064608.
43) J. O. Newton, R. D. Butt, M. Dasgupta, D. J. Hinde, I. I. Gontchar, C. R. Morton and

K. Hagino, Phys. Lett. B **586** (2004), 219; Phys. Rev. C **70** (2004), 024605.
44) A. Mukherjee, D. J. Hinde, M. Dasgupta, K. Hagino, J. O. Newton and R. D. Butt, Phys. Rev. C **75** (2007), 044608.
45) I. I. Gontchar, D. J. Hinde, M. Dasgupta and J. O. Newton, Phys. Rev. C **69** (2004), 024610.
46) K. Hagino, N. Rowley and M. Dasgupta, Phys. Rev. C **67** (2003), 054603.
47) S. Landowne and S. C. Pieper, Phys. Rev. C **29** (1984), 1352.
48) K. Hagino, N. Rowley and A. T. Kruppa, Comp. Phys. Commun. **123** (1999), 143.
49) C. Y. Wong, Phys. Rev. Lett. **31** (1973), 766.
50) Z. E. Switkowski, R. G. Stokstad and R. M. Wieland, Nucl. Phys. A **279** (1977), 502.
51) L. F. Canto, P. R. S. Gomes, J. Lubian, L. C. Chamon and E. Crema, J. of Phys. G **36** (2009), 015109; Nucl. Phys. A **821** (2009), 51.
52) P. R. S. Gomes, J. Lubian and L. F. Canto, Phys. Rev. C **79** (2009), 027606.
53) A. B. Balantekin, S. E. Koonin and J. W. Negele, Phys. Rev. C **28** (1983), 1565.
54) M. W. Cole and R. H. Good, Phys. Rev. A **18** (1978), 1085.
55) M. Inui and S. E. Koonin, Phys. Rev. C **30** (1984), 175.
56) K. Hagino and Y. Watanabe, Phys. Rev. C **76** (2007), 021601(R).
57) S. Yusa, K. Hagino and N. Rowley, Phys. Rev. C **82** (2010), 024606; Phys. Rev. C **85** (2012), 054601.
58) A. Bohr and B. Mottelson, *Nuclear Structure* (Benjamin, New York, 1975), Vol. 2.
59) G. F. Bertsch and R. A. Broglia, *Oscillations in Finite Quantum Systems* (Cambridge University Press, Cambridge, 1994).
60) M. N. Harakeh and A. van der Woude, *Giant Resonances* (Oxford University Press, Oxford, 2001).
61) W. Scobel, A. Mignerey, M. Blann and H. H. Gutbrod, Phys. Rev. C **11** (1975), 1701.
62) T. Rumin, K. Hagino and N. Takigawa, Phys. Rev. C **63** (2001), 044603.
63) K. Hagino and N. Rowley, Phys. Rev. C **69** (2004), 054610.
64) Y. Aritomo, K. Hagino, K. Nishio and S. Chiba, Phys. Rev. C **85** (2012), 044614.
65) A. R. Edmonds, *Angular Momentum in Quantum Mechanics* (Princeton University Press, Princeton, New Jersey, 1960), Eq. (7.1.6).
66) N. Takigawa and K. Ikeda, in *Proc. Symp. Many Facets of Heavy Ion Fusion Reactions*, ed. W. Henning et al. (Argonne National Laboratory Report No. ANL-PHY-87-1), 1986, p. 613.
67) O. Tanimura, Phys. Rev. C **35** (1987), 1600; Z. Phys. A **327**, 413 (1987).
68) H. Esbensen, S. Landowne and C. Price, Phys. Rev. C **36** (1987), 1216; Phys. Rev. C **36** (1987), 2359.
69) A. T. Kruppa, P. Romain, M.A. Nagarajan and N. Rowley, Nucl. Phys. A **560** (1993), 845.
70) J. Gomez-Camacho and R. C. Johnson, J. of Phys. G **12** (1986), L235; J. of Phys. G **14** (1988), 609.
71) K. Hagino, N. Takigawa, M. Dasgupta, D. J. Hinde and J. R. Leigh, Phys. Rev. C **55** (1997), 276.
72) K. Hagino, N. Takigawa and S. Kuyucak, Phys. Rev. Lett. **79** (1997), 2943.
73) K. Hagino, S. Kuyucak and N. Takigawa, Phys. Rev. C **57** (1998), 1349.
74) J. de Boer and J. Eichler, *Advances in Nuclear Physics* (Plenum, New York, 1968), Vol. 1, p. 1.
75) C. H. Dasso, J. Fernández-Niello and A. Vitturi, Phys. Rev. C **55** (1997), 2112.
76) H. Esbensen and S. Landowne, Phys. Rev. C **35** (1987), 2090.
77) A. B. Balantekin, J. R. Bennett and S. Kuyucak, Phys. Rev. C **48** (1993), 1269; Phys. Rev. C **49** (1994), 1079.
78) N. Rowley, in *Proc. Int. Workshop Heavy-Ion Fusion: Exploring the Variety of Nuclear Properties*, ed. A. M. Stefanini et al. (World Scientific, Singapore, 1994), p. 66.
79) A. M. Stefanini et al., Phys. Rev. Lett. **74** (1995), 864.
80) M. W. Kermode and N. Rowley, Phys. Rev. C **48** (1993), 2326.
81) D. M. Brink, *Semi-Classical Methods for Nucleus-Nucleus Scattering* (University Press, Cambridge, 1985).
82) D. M. Brink and U. Smilansky, Nucl. Phys. A **405** (1983), 301.
83) D. M. Brink and N. Takigawa, Nucl. Phys. A **279** (1977), 159.

84) S. Y. Lee, N. Takigawa and C. Marty, Nucl. Phys. A **308** (1978), 161.
85) S. Y. Lee and N. Takigawa, Nucl. Phys. A **308** (1978), 189.
86) K. Hagino and A. B. Balantekin, Phys. Rev. A **70** (2004), 032106.
87) M. A. Nagarajan, N. Rowley and R. Lindsay, J. of Phys. G **12** (1986), 529.
88) M. V. Andres, N. Rowley and M. A. Nagarajan, Phys. Lett. B **202** (1988), 292.
89) N. Takigawa, Y. Alhassid and A. B. Balantekin, Phys. Rev. C **45** (1992), 1850.
90) K. Hagino, N. Takigawa, J. R. Bennett and D. M. Brink, Phys. Rev. C **51** (1995), 3190.
91) H. Esbensen, Phys. Rev. C **68** (2003), 034604.
92) Muhammad Zamrun F.,Zakarya Mohamed Mohamed Mahmoud, N. Takigawa and K. Hagino, Phys. Rev. C **81** (2010), 044609.
93) H. Timmers, M. Dasgupta, D. J. Hinde, J. R. Leigh, R. C. Lemmon, J. C. Mein, C. R. Morton, J. O. Newton and N. Rowley, Nucl. Phys. A **584** (1994), 190.
94) C. R. Morton, M. Dasgupta, D. J. Hinde, J. R. Leigh, R. C. Lemmon, J. P. Lestone, J. C. Mein, J. O. Newton, H. Timmers, N. Rowley and A. T. Kruppa, Phys. Rev. Lett. **72** (1994), 4074.
95) K. Hagino, N. Takigawa and A. B. Balantekin, Phys. Rev. C **56** (1997), 2104.
96) O. Tanimura, J. Makowka and U. Mosel, Phys. Lett. B **163** (1985), 317.
97) A. B. Balantekin and N. Takigawa, Ann. of Phys. **160** (1985), 441.
98) N. Takigawa, K. Hagino, M. Abe and A. B. Balantekin, Phys. Rev. C **49** (1994), 2630.
99) K. Hagino, N. Takigawa, M. Dasgupta, D. J. Hinde and J.R. Leigh, Phys. Rev. Lett. **79** (1997), 2014.
100) C. L. Jiang et al., Phys. Rev. Lett. **89** (2002), 052701; Phys. Rev. Lett. **93** (2004), 012701.
101) C. L. Jiang et al., Phys. Rev. C **71** (2005), 044613; Phys. Rev. C **78** (2008), 017601; Phys. Rev. C **81** (2010), 024611.
102) A. M. Stefanini et al., Phys. Rev. C **78** (2008), 044607; G. Montagnoli et al., Phys. Rev. C **82** (2010), 064609.
103) C. L. Jiang et al., Phys. Rev. C **82** (2010), 041601(R); G. Montagnoli et al., Phys. Rev. C **85** (2012), 024607.
104) M. Dasgupta et al., Phys. Rev. Lett. **99** (2007), 192701.
105) S. Misicu and H. Esbensen, Phys. Rev. Lett. **96** (2006), 112701; Phys. Rev. C **75** (2007), 034606.
106) C. H. Dasso and G. Pollarolo, Phys. Rev. C **68** (2003), 054604.
107) T. Ichikawa, K. Hagino and A. Iwamoto, Phys. Rev. C **75** (2007), 057603; Phys. Rev. Lett. **103** (2009), 202701.
108) T. Ichikawa, K. Hagino and A. Iwamoto, Phys. Rev. Lett. **103** (2009), 202701.
109) C. L. Jiang, H. Esbensen, B. B. Back, R. V. F. Janssens and K. E. Rehm, Phys. Rev. C **69** (2004), 014604; C. L. Jiang, B. B. Back, H. Esbensen, R. V. F. Janssens and K. E. Rehm, Phys. Rev. C **73** (2006), 014613.
110) T. Ichikawa, K. Hagino and A. Iwamoto, Phys. Rev. C **75** (2007), 064612.
111) E. S. Z. Thein, N. W. Lwin and K. Hagino, Phys. Rev. C **85** (2012), 057602.
112) M. Evers et al., Phys. Rev. C **84** (2011), 054614.
113) A. Diaz-Torres, D. J. Hinde, M. Dasgupta, G. J. Milburn and J. A. Tostevin, Phys. Rev. C **78** (2008), 064604.
114) B. V. Carlson, O. Civitarese, M. S. Hussein and A. Szanto de Toledo, Ann. of Phys. **169** (1986), 167.
115) D. Hahn, G. Terlecki and W. Scheid, Nucl. Phys. A **325** (1979), 283.
116) S. Mukamel, U. Smilansky, D. H. E. Gross, K. Möhring and M. I. Sobel, Nucl. Phys. A **366** (1981), 339.
117) D. H. E. Gross, K. Möhring, S. Mukamel, U. Smilansky and M. I. Sobel, Nucl. Phys. A **378** (1982), 375.
118) J. Blocki, Y. Boneh, J. R. Nix, J. Randrup, M. Robel, A. J. Sierk and W. J. Swiatecki, Ann. of Phys. **113** (1978), 330.
119) J. Randrup, Ann. of Phys. **171** (1986), 28.
120) T. Dossing and J. Randrup, Nucl. Phys. A **475** (1987), 557.
121) G. R. Darling and S. Holloway, Rep. Prog. Phys. **58** (1995), 1595, and references therein.
122) B. Hammer, M. Scheffler, K. W. Jacobsen and J. K. Nørskov, Phys. Rev. Lett. **73** (1994), 1400.
123) C. T. Rettner, D. J. Auerbach and H. A. Michelsen, Phys. Rev. Lett. **68** (1992), 1164.

124) H. A. Michelsen, C. T. Rettner and D. J. Auerbach, Phys. Rev. Lett. **69** (1992), 2678.
125) H. A. Michelsen, C. T. Rettner, D. J. Auerbach, and R. N. Zare, J. Chem. Phys. **98** (1993), 8294.
126) W. Brenig and H. Kasai, Surf. Sci. **213** (1989), 170.
127) H. Kasai and A. Okiji, Prog. Surf. Sci. **44** (1993), 101.
128) Y. Chiba and W. Brenig, Surf. Sci. **306** (1994), 406.
129) W. A. Diño, H. Kasai and A. Okiji, J. Phys. Soc. Jpn.**64** (1995), 2478; Phys. Rev. Lett. **78** (1997), 286.
130) W. A. Diño, H. Kasai and A. Okiji, Surf. Sci. **363** (1996), 52.
131) W. A. Diño, H. Kasai and A. Okiji, Prog. Surf. Sci. **63** (2000), 63.
132) Y. Miura, H. Kasai and W. A. Diño, J. Phys. Soc. Jpn. **68** (1999), 887.
133) A. Gross, S. Wilke and M. Scheffler, Phys. Rev. Lett. **75** (1995), 2718.
134) W. A. Diño, private communication.
135) M. S. Hussein, M. P. Pato, L. F. Canto and R. Donangelo, Phys. Rev. C **46** (1992), 377.
136) N. Takigawa, M. Kuratani and H. Sagawa, Phys. Rev. C **47** (1993), R2470.
137) C. H. Dasso and A. Vitturi, Phys. Rev. C **50** (1994), R12.
138) K. Hagino, A. Vitturi, C. H. Dasso and S. M. Lenzi, Phys. Rev. C **61** (2000), 037602.
139) A. Diaz-Torres and I. J. Thompson, Phys. Rev. C **65** (2002), 024606.
140) M. Ito, K. Yabana, T. Nakatsukasa and M. Ueda, Phys. Lett. B **637** (2006), 53.
141) P. R. S. Gomes, L. F. Canto, J. Lubian and M. S. Hussein, Phys. Lett. B **695** (2011), 320.
142) D. H. Luong, M. Dasgupta, D. J. Hinde, R. du Rietz, R. Rafiei, C. J. Lin, M. Evers and A. Diaz-Torres, Phys. Lett. B **695** (2011), 105.
143) M. Dasgupta et al., Phys. Rev. Lett. **82** (1999), 1395; Phys. Rev. C **66** (2002), 041602; Phys. Rev. C **70** (2004), 024606.
144) R. Raabe et al., Nature **431** (2004), 823.
145) C. Signorini et al., Nucl. Phys. A **735** (2004), 329.
146) A. Lemasson et al., Phys. Rev. Lett. **103** (2009), 232701.
147) J.F. Liang et al., Phys. Rev. C **85** (2012) 031601(R).
148) M. Alcorta et al., Phys. Rev. Lett. **106** (2011), 172701.
149) A. Lemasson et al., Phys. Lett. **B697** (2011), 454.
150) R. Rafiei, R. du Rietz, D. H. Luong, D. J. Hinde, M. Dasgupta, M. Evers and A. Diaz-Torres, Phys. Rev. C **81** (2010), 024601.
151) Z. Kohley et al., Phys. Rev. Lett. **107** (2011), 202701.
152) P. H. Stelson, Phys. Lett. B **205** (1988), 190.
153) N. Rowley, I. J. Thompson and M. A. Nagarajan, Phys. Lett. B **282** (1992), 276.
154) H. Esbensen, C. L. Jiang and K.E. Rehm, Phys. Rev. C **57** (1998), 2401.
155) N. Rowley, in *Proc. Fusion Dynamics at the Extremes, Dubna, 2000*, ed. Yu. Ts. Oganessian and V.I. Zagrebaev (World Scientific, Singapore, 2001), p. 297.
156) G. Pollarolo and A. Winther, Phys. Rev. C **62** (2000), 054611.
157) V. I. Zagrebaev, Phys. Rev. C **67** (2003), 061601.
158) J. Bardeen, Phys. Rev. Lett. **6** (1961), 57.
159) P. Ring and P. Schuck, *The Nuclear Many Body Problem* (Springer-Verlag, New York, 1980).
160) C. Simenel, D. Lacroix and B. Avez, *Quantum Many-Body Dynamics: Applications to Nuclear Reactions* (VDM Verlag, Sarrebruck, Germany, 2010).
161) A. Bonasera and V. N. Kondratyev, Phys. Lett. B **339** (1994), 207.
162) V. N. Kondratyev, A. Bonasera and A. Iwamoto, Phys. Rev. C **61** (2000), 044613.
163) S. Kimura, N. Takigawa, M. Abe and D. M. Brink, Phys. Rev. C **67** (2003), 022801(R).
164) N. Takigawa, K. Hagino and M. Abe, Phys. Rev. C **51**(1995), 187.
165) A. S. Umar and V. E. Oberacker, Phys. Rev. C **76** (2007), 014614; Phys. Rev. C **77** (2008), 064605.
166) V. E. Oberacker, A. S. Umar, J. A. Maruhn and P.-G. Reinhard, Phys. Rev. C **82** (2010), 034603; Phys. Rev. C **85** (2012), 034609.
167) R. Keser, A. S. Umar, and V. E. Oberacker, Phys. Rev. C **85** (2012), 044606.
168) L. V. Grigorenko et al., Phys. Rev. C **64** (2001), 054002.
169) L. V. Grigorenko et al., Phys. Rev. C **80**(2009), 034602.
170) M. Pfützner, M. Karny, L. V. Grigorenko and K. Riisager, Rev. Mod. Phys. **84** (2012),

567.
171) B. Blank and M. Ploszajczak, Rep. Prog. Phys. **71** (2008), 046301.
172) L. V. Grigorenko, Phys. Part. Nucl. **40** (2009), 674, and references therein.
173) T. Maruyama, T. Oishi, K. Hagino and H. Sagawa, Phys. Rev. C **86** (2012), 044301.
174) D. S. Delion, *Theory of particle and cluster emission* (Springer-Verlag, Berlin, 2010).
175) K. Sasaki, K. Suekane and I. Tonozuka, Nucl. Phys. A **147** (1970), 45.
176) I. Tonozuka and A. Arima, Nucl. Phys. A **323** (1979), 45.
177) K. Varga and J. Liotta, Phys. Rev. C **50** (1994), R1292.
178) R. Id Betan and W. Nazarewicz, Phys. Rev. C **86** (2012), 034338.
179) N. Poffe, N. Rowley and R. Lindsay, Nucl. Phys. A **410** (1983), 498.
180) A. Kabir, M. W. Kermode and N. Rowley, Nucl. Phys. A **481** (1988), 94.
181) H. Esbensen, Phys. Rev. C **85** (2012), 064611.
182) P. Sperr et al., Phys. Rev. Lett. **37** (1976), 321; D.G. Kovar et al., Phys. Rev. C **20** (1979), 1305.
183) I. Tserruya et al., Phys. Rev. C **18** (1978), 1688.
184) A. B. Balantekin, A. J. DeWeerd and S. Kuyucak, Phys. Rev. C **54** (1996), 1853.